Atypical Cell Cycle Regulation over Neural Stem Cell Expansion

Ingrid Qemo*, Dorota Lubanska*, Keith Franklin Stringer, Bre-Anne Fifield, Youshaa Elabed, Hema Priya Mahendran, Sami Alrashed, Emmanuel Boujeke, Alexander Rodzinka, Alexandra Sorge, Srinath Kandalam, Jillian Brown, Hasan Ghafoor, Maheen Arshad, Lisa A. Porter [£]

*Contributed equally

[£] Corresponding author:
University of Windsor Ontario
Windsor, ON N9B 3P4
Phone: (519) 253-3000 x4775
Fax: (519) 571-3609
lporter@uwindsor.ca

SUMMARY

Populations of quiescent adult neural stem cells (NSCs) that reside in the mammalian brain aid in neurogenesis throughout life and can be identified by molecular markers including Nestin, a type VI intermediate filament protein. Cell cycle regulation plays an important role in determining the fate of NSCs in the adult brain and maintaining a crucial balance between self-renewal and differentiation. Data from our group and others support that the atypical cyclin-like protein Spy1 (also called RingoA; gene *SPDYA*) plays a critical role in activating NSCs from a quiescent state. Elevated levels of Spy1 are found in aggressive human brain cancers, including glioblastoma. Using a conditional mouse model, we demonstrate that driving the expression of Spy1 in the Nestin-enriched NSC population of the brain directs the cells toward symmetric cellular division, increases stemness characteristics, decreases differentiation, and increases susceptibility to oncogenic transformation & drug resistance. This study contributes to better understanding of intricate cell cycle mechanisms which lead to deviation from the homeostatic state, promoting aberrant changes in adult NSCs.

INTRODUCTION

Neurogenesis is the process by which new neurons and glial cells are formed in the brain. This phenomenon occurs primarily during embryonic development, but it also persists to a limited extent in the adult brain in select neurogenic niches including the lateral ventricles of the subventricular zone (SVZ), and dentate gyrus of the subgranular zone (SGZ) [1, 2]. Neurogenesis dictates normal brain development, brain plasticity, cognitive function, memory, emotional regulation, and regenerative capacity of the brain. Abnormal neurogenesis can manifest across a spectrum of developmental, neurological, and psychiatric outcomes and may support susceptibility to neurodegenerative and/or neuroproliferative diseases and syndromes including carcinogenesis.

Long-lived neural stem cells (NSC) possess the remarkable ability to self-renew and differentiate into all of the functional cell types within the brain. Molecular biomarkers have been used in attempt to unambiguously categorize NSCs and their progeny in the adult SVZ. Nestin is one marker of NSCs and transient amplifying cell populations (progenitor cells) of the SVZ [3]. Data suggests that Nestin is necessary for NSC self-renewal and survival [4]. Nestin-positive cells are exclusively found in regions of the brain that harbor a niche tailored to the maintenance of stem and progenitor populations [5] where NSCs are maintained in a state of quiescence [6].

Mechanistically, NSCs respond to environmental and extracellular stimuli, growth factors, cytokines, and cues from the niche and surrounding microenvironment to trigger neurogenesis. During embryonic development NSCs are in a constant state of self-renewal and differentiation with a cell cycle length of only ~8 hours, however adult NSCs increase the length of the cell cycle dramatically with up to a 4-fold increase in G1

phase of the cell cycle, and as adults assume a state of quiescence to preserve their population [7, 8.] Triggering of neurogenesis in adult NSCs requires exiting quiescence and re-entering the cell cycle [9]. The tumor suppressor p53 is upregulated in the quiescent neurogenic niches of the brain where it maintains an equilibrium between self-renewal and differentiation regulating activity of the G1/S Cyclin Dependent Kinase (CDK), CDK2 [10]. Inactivation of p53 results in an activation of quiescent stem cells and an expansion of NSCs [11, 12, 13]. Loss/inactivation of p53 is found in many human tumours and is attributed to boosting the stemness properties of cancer cells contributing to aggressive, drug resistant disease [14, 15, 16].

Spy1 protein (gene *SPDYA*; also called RingoA) directly binds to, and activates, both CDK1 and CDK2 in a unique fashion that is independent of activating phosphorylation and dephosphorylation events [15, 16]. As a result of this mechanism Spy1 has been isolated from numerous screens and has been described for the ability to override cell cycle arrest mechanisms including DNA damage and cellular senescence [19, 20]. Data from our lab show that Spy1 can enhance pluripotent reprograming by epigenetic downregulation of CDK inhibitors and is essential for overcoming reprogramming-induced senescence [21]. Work from the Nebreda lab has recently demonstrated that Spy1 is required for activation of NSCs out of quiescent state via activation of CDK2 [22]. The authors showed that brains of mice deficient in Spy1 have decreased neurogenesis and accumulate quiescent cell populations [22]. Our lab has also shown that in mammary progenitors, Spy1 plays an important role during normal development, and Spy1 protein levels accumulate to inhibit differentiation [23]. Spy1 levels elevate following acute sciatic nerve injury, suggesting a potential role in CNS regeneration [24]. Endogenous levels of

Spy1 are elevated in several types of cancer [25, 26, 27] and Spy1 regulates symmetric division and expansion of aggressive populations of brain tumour initiating cells in human glioma[28]. Mechanistically, the Spy1-CDK complex overrides the inhibitory effects of downstream p53 targets, p27 and p21 [20] and work from our lab has demonstrated that p53 targets Spy1 for degradation in breast and immortalized cell lines [29]. Hence, the literature supports that p53 holds the Spy1 protein in check in select systems. Whether Spy1 alone can override the protective effects of p53 in NSCs and drive phenotypes resembling a brain-targeted p53 null mouse is an interesting question that we sought to address.

Using a conditional mouse model this work characterises the consequence of elevated Spy1 protein levels in Nestin-positive populations in the mammalian brain. We show that Spy1 delays neuronal differentiation, promotes symmetric expansion of NSCs and increases susceptibility to oncogenic transformation *in vitro*, mimicking the neural phenotypes seen with loss of p53 [30]. We further provide data to support that select drivers of glioma rely on endogenous Spy1 to maintain tumour progression *in vivo*. This work contributes to better understanding of the cell cycle mechanisms capable of tipping the balance of decisions in NSCs capable of predisposing this population of cells toward supporting oncogenesis.

RESULTS

Construction and generation of pTRE-Spy1 transgenic mouse

To address the role of Spy1 in NSC populations of the mammalian brain, we generated a transgenic mouse system, termed NTA-Spy1, which permits inducible, spatially homogenous expression of Spy1 throughout the course of development as originally

described by the Chodosh group [31]. This mouse model has uniquely allowed the control of Spy1 under the Nestin promoter. The Flag-Spy1 sequence was removed from a previously described vector – Flag-Spy1A-pLXSN and was cloned into a pTRE-Tight-Caspase3 vector backbone (Figure S1A). A restriction digest using XhoI and AlwNI was performed to remove the 536bp portion of the plasmid that was used for microinjection (Figure S1B). PCR analysis depicted pTRE-Spy1 positive founder mice through the presence of a 536bp band (Figure S1C). The pTRE-Spy1 mice express the open reading frame of Spy1 downstream of a promoter containing a series of tetracycline operator sequences. Lastly, the positive founder mice of a B6CBAF1/J background were found to transmit the pTRE-Spy1 transgene to their progeny (Figure S1D).

Generation and characterization of the NTA-Spy1 transgenic mouse

To create the NTA-Spy1 mouse, pTRE-Spy1 transgenic mice were crossed with Nestin-rtTA mice (Figure 1A). This ensured that Spy1 would be expressed under the Nestin promoter in the presence of doxycycline. Nestin is an intermediate filament protein that begins to accumulate in the neural precursor cells of the brain at embryonic day 12 (E12) and is retained in NSC populations throughout adult life [32]. NSCs comprise a very small population of the brain and are in unique areas, one of which is the SVZ. Post-natal (PN) day 2 brains were micro-dissected to remove the SVZ. Extracted cells from the SVZ were cultured in the presence or absence of doxycycline and qRT-PCR was performed for Flag and Spy1 mRNA expression in the NTA-Spy1 and all other littermate controls. NTA-Spy1 mice show significant increase in Flag and Spy1 expression in the presence of doxycycline as compared to littermate controls (Figure 1B). Primary cells harvested from the SVZ were also used for western blot analysis. NTA-Spy1 doxycycline-treated NSCs

showed an increase in Spy1 protein when compared to NTA-Spy1 cells not treated with doxycycline as well as pTRE-Spy1 littermate controls with or without doxycycline. A representative western blot (left) has been shown and protein levels were measured in relative units for densitometry values (right) (Figure 1C). To determine if Spy1 levels were being upregulated specifically in the Nestin positive population, mouse SVZ were dissected and subjected to fluorescence associated cell sorting for Nestin. The positive and negative Nestin cell populations from both the NTA-Spy1 and littermate control pTRE-Spy1 mice were analyzed through qRT-PCR for Spy1 levels (Figure 1D). There was a significant increase in Spy1 levels within each genotype when comparing the Nestin positive and negative populations. There was also a significant increase in Spy1 levels between the Nestin positive populations between NTA-Spy1 and pTRE-Spy1.

Enhanced proliferation and NSC expansion in NTA-Spy1 mice

Transient overexpression of Spy1 in wildtype NSCs extracted from the SVZ reveals an increase in gene expression levels of key stem cell markers Musashi 1 (Msi1), CD133, Bmi1, Vimentin and Nestin as compared to empty vector control (Figure S2). This supports a role for Spy1 levels in regulating stemness properties of NSCs. To assess the consequence of elevated Spy1 levels in the NSC population of the NTA-Spy1 mice, we performed SVZ cell extractions from NTA-Spy1 mouse brains along with their littermate controls. NTA-Spy1 derived NSCs presented elevated levels of proliferation in culture in comparison to all controls as assessed by a BrdU incorporation assay (Figure 2A). The percent of BrdU positive cells was calculated as BrdU+ cells over the total cell population (right). NTA-Spy1 cells had a significantly higher percentage of BrdU+ cells compared to all other control cells. Neurosphere formation assays correlate with *in vivo*

self-renewal and proliferation of NSCs [33, 34]. A neurosphere formation assay (Figure 2B) revealed that NTA-Spy1 cells form significantly more spheres over serial passages (Figure 2B; left), and that neurospheres are generally larger in size (Figure 2C) as compared to controls, suggesting enhanced stemness and proliferation among NTA-Spy1 derived NSCs.

A limitation of the neurosphere formation assay is that it does not have the capacity to discriminate between spheres that were derived from single cells versus spheres that have formed due to an aggregation of cells. The clonality self-renewal assay, in which neurospheres are dissociated and seeded as single cells in 96-well low attachment plates, circumvents this limitation. When we performed a single cell self-renewal assay, we showed that NTA-Spy1 cells had a higher proportion of self-renewing NSCs (Figure 2D). NTA-Spy1 also had a significant increase in gene expression for stemness markers CD133, Sox2 and Nestin throughout serial passaging (Figure 2E). In addition, densitometric analysis of protein expression revealed that Sox2 protein levels, were significantly elevated in the NTA-Spy1 NSC population as compared to pTRE-Spy1 cells (Figure S3A).

Interestingly, upon further investigation of reprogramming transcription factor genes Oct4, Sox2, c-Myc, Klf4 and Nanog [35, 36], qRT-PCR analysis revealed that NTA-Spy1 cells have upregulated levels of reprogramming gene expression as compared to pTRE-Spy1 littermate controls (Figure 2F). We then tested the gene expression levels of defined reprogramming transcription factors essential for propagating tumour initiating cells from differentiated progeny [37]. We found increases of all stemness factors in cells derived from NTA-Spy1 mouse in comparison to pTRE-Spy1 control (Figure S3B). Due

to an intrinsic increase in reprogramming genes, we wanted to determine whether NTA-Spy1 cells had the potential to sustain self-renewal regardless of being cultured in differentiation promoting media. We employed a re-sphering assay, as previously described [38]. We dissociated neurospheres that had grown in EGF and FGF-containing media and plated single cells at 400 cells per well on 96-well plates in 2% FBS containing media to promote differentiation (Figure S3C). Initially, we observed cell differentiation and there was no visible sphere formation, however, new neurospheres started appearing in the differentiation conditions 2 weeks post-differentiation. A higher percentage of cells generated spheres in the NTA-Spy1 cohort as compared to pTRE-Spy1 controls (Figure S3D; left). The re-sphered cells remained attached in 2D during the span of the differentiation experiment (Figure S3D; right). qRT-PCR analysis of differentiation markers S-100β (astrocyte marker), Foxo4 (O4) (oligodendrocyte marker), and Mapt (neuronal marker) show an increase during differentiation compared to initial neurospheres and decreased in the newly formed spheres compared to differentiated cells (Figure S3E). Interestingly, NTA-Spy1 cells had significantly lower expression of all differentiation markers throughout all stages relative to the pTRE-Spy1 control. This suggests that the cells that were capable of re-sphering were primed for this prior to being subjected to differentiation. We were able to remove and dissociate individual spheres and plate them back into neurosphere culture where they were able to continue expanding as 3D floating neurospheres.

NTA-Spy1 mice exhibit decreased neural differentiation capacity

NSCs that are taken out of EGF and FGF-containing neurosphere cultures in the presence of FBS will start to differentiate. To determine the effect of increased levels of Spy1 on

NSC lineage differentiation, we cultured NSCs in adherent conditions in the presence of 2% FBS without growth factors to induce differentiation. Morphology was used to score differentiated cells at the indicated time points. Cells that contained outgrowth processes of at least two cell-body diameters in length were scored as differentiated. We found that NTA-Spy1 cells had a significant decrease in differentiation potential compared to control littermates, as can be seen in representative images (right) and scored percentage of differentiated cells (left) (Figure 3A). To distinguish if there was a neural differentiation lineage that may have been impaired more than others, we used differentiation protocols to drive the NSCs down astrocyte, oligodendrocyte, or neuronal lineages. NSCs were plated on polyornithine coated dishes and given different supplements in their respective mediums. Gene expression of S-100β, O4, Beta III tubulin (neuronal marker) as well as Mapt was analyzed via qRT-PCR at 0, 48 and 96 hours of the differentiation time course (Figure 3B). Although NTA-Spy1 cells show a decrease in differentiation capacity to astrocyte and oligodendrocyte lineages, the biggest and most significant effect was seen in the neuronal lineage. NTA-Spy1 cells have an early decrease in neuronal differentiation capacity compared to control pTRE-Spy1 cells. The CDK inhibitor p27 enhances neural differentiation and we have previously shown that Spy1-CDK actively targets p27 for degradation [39, 40, 41, 42]. Hence, prior to the commencement of differentiation, protein expression of p27 was analyzed in pTRE-Spy1 and NTA-Spy1 cells through western blotting. We found that there was significantly less p27 protein in NTA-Spy1 compared to pTRE-Spy1 controls (Figure 3C). These experiments demonstrate that Spy1-mediated effects on neuronal differentiation occur

concomitant with an activation of cell cycle progression and a reduction in p27 degradation.

NTA-Spy1 NSC shift towards Musashi 1-mediated symmetric mode of division

We have previously demonstrated that Spy1 drives expansion of human glioma stem cells through regulating their mode of division [28]. Asymmetric cell division supports the terminal differentiation identity of neurons in *C. elegans* [44]. In *Drosophila* and mice, the basic molecular mechanism of asymmetric cell division involves the subcellular localization of cell fate determining protein Numb [45, 46, 47, 48]. To assess the impacts of NTA-Spy1 on cell fate in the presence of signals from the extracellular matrix, pTRE-Spy1 and NTA-Spy1 cells were cultured at low densities in Matrigel. Elevated Spy1 levels resulted in over 3-fold increase in the number of 3D colonies that were formed and a significant decrease in the percentage of differentiated cells (Figure 4A). To determine any changes in mode of division in the NTA-Spy1 mice, we performed a clonal assay in MaxGel ECM and monitored the distribution of Numb between mitotic cell pairs. NTA-Spy1 cells presented with increased symmetric distribution of Numb protein (Figure 4B; left), indicative of an increase in symmetric division. Analysis of mitotic cell pairs with symmetric and asymmetric Numb distribution over the total cell pairs was performed (Figure 4B; right) and verified the significant increase in symmetric cell division and a decrease in asymmetric division in NTA-Spy1 cell as compared to control littermate pTRE-Spy1.

The Notch pathway plays a vital role in NSC maintenance and self-renewal [49–51] (Figure 4C). Notch expression is regulated by Numb and Musashi l (Msi1) [52]. Msi1 activation and function is directly induced through phosphorylation by Spy1-bound

CDK2 [53]. Western blot analysis (Figure 4D; left) revealed that Msi1 protein levels are increased in NTA-Spy1 cells as compared to pTRE-Spy1 (Figure 4D). This corresponded to significantly decreased levels of Numb protein (Figure 4D). To test whether Msi1 plays a role in Spy1-mediated symmetry of division, we used short interference RNA (siRNA) against Msi1. qRT-PCR analysis confirmed a significant decrease in Msi1 mRNA levels and a decrease in Notch transcriptional targets, *Hes1* and *Hes5,* downstream of Msi1 (Figure 4E). We performed a clonal assay to determine whether the increased symmetric division seen in NTA-Spy1 cells was mediated through the Msi1 pathway. When we use siMsi1 we find that there is a decrease in symmetric cell division in NTA-Spy1 cells bringing levels to that which is comparable to pTRE-Spy1 control cells (Figure 4F). This suggests that Spy1 is increasing symmetric cell division in NTA-Spy1 cells through the Msi1 signaling pathway.

Aging NTA- Spy1 mice retain NSCs and present impaired cognitive functions

To characterize the capacity of NTA-Spy1 mice to maintain the pools of NSCs we tested the Nestin+ population of cells in aging NTA-Spy1 mice. The neurogenic regions of the brain were dissected from 20-month-old mice. Cells derived from NTA-Spy1 mice showed not only significantly increased proliferation in comparison to controls as assessed by BrdU incorporation assay (Figure 5A) but continued to demonstrate a block in differentiation at each time point tested in aging primary Nestin+ cells (Figure 5B). Staining of the brain sections obtained from 20-month-old mice with PCNA revealed upregulation of the number of PCNA+ cells in NTA-Spy1 mice in comparison to control mice (Figure 5C). In addition, NTA-Spy1 cells showed increased mRNA levels of the proliferation marker Ki67 (Figure 5D), as well as decreased levels of CKI gene

expression of p21 (*Cdkn1a*), INK4 (*Cdkn2a*), and p53 (*Trp53*) (Figure 5E) as compared to pTRE-Spy1 cells. Histone γH2A.X is the most common marker for DNA double strand breaks and telomere shortening [54, 55], and at times can also be used as a cellular senescence marker [56]. Notably, when we performed immunofluorescence for γH2A.X foci we found that NTA-Spy1 cells had a decrease in the number of γH2A.X foci compared to control littermates (Figure 5F). We also found a decrease in apoptosis as measured by Caspase 3/7 activity in the NTA-Spy1 cells compared to pTRE-Spy1 controls (Figure 5G). This suggests that Nestin+ cells of NTA-Spy1 aging mice continue to proliferate with no signs of NSC pool depletion by any means.

To determine how the observed blockage in differentiation affects neuronal layering along the cortex, we stained sections with a neuron specific stain, Nissl, and scored Nissl+ cells. NTA-Spy1 mice showed a shift in neuronal positioning of the cortical plate (Figure 5H) with obvious accumulation of neuronal bodies in closer proximity to ventricular zone as compared to Nestin-rtTA control mice, suggesting the role of Spy1 in controlling differentiation timing during development. Finally, we sought to establish if the observed changes to neuronal positioning were affecting cognitive functions in mice. We performed the novel object recognition task, as demonstrated by the schematic (Figure 5I; top). Interestingly, NTA-Spy1 mice had significantly decreased preference for novel objects brought to the task set up as compared to their littermate controls (Figure 5I; bottom). In summary, upregulation of Spy1 levels in Nestin+ cells results in abnormal positioning of neurons and impairs cognitive functions in NTA-Spy1 mice.

Spy1 increases proliferation of transformed NSCs

Given the established role of Spy1 in several types of cancer including malignancies of neural origin, we were interested in investigating whether the elevated levels of Spy1 in the NTA mice would contribute to transformation of NSCs in face of applied pro-oncogenic changes. We first studied the effects of Spy1 overexpression on the expression pattern of selected tumour suppressor genes in the mouse brain through immunostaining of the brain sections of NTA-Spy1 mice versus control with antibodies against p53 and PTEN. We found upregulated expression of p53 in the cells of the hippocampus of NTA-Spy1 mice, while no difference was observed in cells of the subventricular zone or cortex (Figure 6A). Our results revealed a significant increase of Pten expression in the hippocampus and cortex of NTA-Spy1 mice compared to control, with no difference observed in the subventricular zone (Figure 6B). These findings suggest that NTA-Spy1 mice exhibit molecular changes associated with a response to counteract potential pro-oncogenic effects of Spy1. To further explore the importance of Spy1 in potentially aberrant changes in NSC populations, we downregulated the levels of p53 and inhibited Pten using shRNA and bpV(HOpic), PTEN inhibitor (PTENi), respectively, in primary cultures from NTA-Spy1 and control pTRE-Spy1 mice (Figure S4A & B). Gene expression analysis revealed that there was an overall significant increase in Cyclin D1 and c-Myc levels in the NTA-Spy1 in comparison to the pTRE-Spy1 cultures (Figure 6C). The expression levels of selected targets were further elevated with downregulation of p53 and inhibition of Pten individually and in combination in NTA-Spy1 derived cells compared to the pTRE-Spy1 control (Figure 6C). This data supports that overexpression of Spy1 protein levels correlate with alterations in other genes/proteins associated with increasing proliferation and stemness found in brain malignancies.

Spy1 enhances oncogenic transformation in NSCs in the presence of selected aberrant events

A hallmark characteristic of oncogenic transformation is the ability to survive and proliferate in low attachment conditions (Figure S5A) [57]. Cultures derived from NTA-Spy1 or pTRE-Spy1 mice were transduced with shp53, RasV12, using lentivirus, and treated with PTENi or vehicle control in the presence and/or absence of doxycycline and subjected to low attachment conditions using ultra-low attachment plates for five days. Viability was assessed using 3D Cell Titer Glo assay and revealed that pTRE-Spy1 littermate controls had significantly higher viability when grown in attachment conditions, consistent with the growth preference of non-transformed cells (Figure S5B, top). However, NTA-Spy1 cells exhibited similar viability in both growth conditions (Figure S5B, bottom), suggesting enhanced survival capacity of NTA-Spy1 cultures in non-adherent conditions as compared to littermate controls. The viability of NTA-Spy1 cultures is significantly enhanced in ultra-low attachment conditions in the presence of overexpression of RasV12 and/or combined with the treatment with PTENi and siRNA against p53 (Figure S5D), this was not seen with inhibition/knockdown of PTEN or p53 alone (Figure S5C). This supports the hypothesis that NTA-Spy1 cells are more susceptible to oncogenic transformation. To further explore this result, we conducted classical soft agar colony formation assay in NTA-Spy1 cells compared to pTRE-Spy1 controls with combined attenuation of p53 and PTEN. At 21 days post-seeding, transformation potential of the cells was assessed by scoring the colonies with a diameter equal to or greater than 50 microns. A significantly higher number of colonies were generated from NTA-Spy1 cells in comparison to cells from the pTRE-Spy1 control

(Figure 7A). There was also a significant increase in the number of colonies in the NTA-Spy1 in comparison to pTRE-Spy1 upon p53 knockdown and PTENi treatment, alone. Significant increase in the number of colonies was observed in NTA-Spy1 NSCs which had both the shp53 and PTENi combined (Figure 7A). We then conducted a colony formation assay using NTA-Spy1 and pTRE-Spy1 cells transduced with RasV12 and/or control. Although the overexpression of Ras resulted in colonies forming regardless of Spy1 overexpression, the NTA-Spy1 NSCs generated significantly more colonies that pTRE-Spy1 cells (Figure 7B). The significant increase in transformation potential of NTA-Spy1 cells compared to pTRE-Spy1 control are consistent with the suggestion that elevated Spy1 levels facilitate the path toward oncogenic transformation. To address the capacity of NTA-Spy1 to support tumour formation, we made use of a zebrafish xenograft model. NTA-Spy1 cells or littermate pTRE-Spy1 controls, with or without sip53, were engrafted into zebrafish larvae at 48 hours post fertilization (hpf) and the number of resulting foci per larvae was scored 4 days after injection (Figure 7C, left). There was a significant increase in foci formation in sip53 NTA-Spy1 cells over sip53 pTRE-Spy1 control (Figure 7C, right), notably sip53 also increased foci in all conditions over control as one would expect. To investigate the importance of Spy1 in brain tumourigenesis in a murine model, GL261 mouse glioma cells driven by p53 and Ras mutations, were transduced with shRNA against Spy1 or a scrambled control. The cells were transplanted orthotopically into neonatal C57BL/6 mice of syngeneic background. 14 days post injection 7/8 mice injected with the control developed visible tumours whereas tumours from shSpy1 cells were found in 4/8 mice at the 14-day timepoint (Figure 7D, left). Analysis of the tumour burden at 15 days post injection showed

significantly downregulated brain tumour size in mice injected with shSpy1 cells when compared to the scrambled control (Figure 7D, right). The data shows that Spy1 not only cooperates with known aberrant changes found in glioma to induce tumourigenesis in normal NSCs but also contributes to proliferation/growth in tumours driven by the selected mutations.

It has previously been shown that Spy1 overrides the DNA damage response in a variety of other cell types [58, 59, 60, 29]. To determine whether NTA-Spy1 NSCs have altered response to DNA damage cells were treated with the standard of care chemotherapy relied upon in the treatment of many neural tumours, temozolomide (TMZ). NTA-Spy1 cells demonstrated significantly lower levels of apoptosis as measured by Caspase 3/7 activity assay in comparison to Nestin-rtTA control cells (Figure 7E, left). The treatment resistance was further enhanced in NTA-Spy1 NSCs when p53 knockdown was introduced (Figure 7E, right). Overexpression of RasV12 in the NTA-Spy1 cells further increased resistance to cell cycle arrest mediated by a synthetic CKI, NU2058, and/or TMZ, alone and in combination (Figure 7F).

DISCUSSION

In normal brain it is accepted that proliferative cell cycle genes support the expansion of the NSC pool while limiting successful neurogenesis [61, 20]. Much less understood is how NSCs balance cell cycle states such as quiescence to maintain homeostasis. A study by Gonzalez *et al*. demonstrated the essentiality of the atypical cell cycle regulator Spy1 in the activation of NSC pools from the quiescent state followed by decreased neurogenesis [22], the molecular mechanisms by which Spy1 regulates the NSC pool in the normal adult brain remain fundamentally unknown. In human CD133+ brain tumour initiating cells

derived from glioma patients, symmetric division regulated by Spy1 is critical for clonal expansion of this cell population [28]. This study established the NTA-Spy1 mouse model which permits spatial control of the expression of Spy1 under the Nestin promoter allowing for detailed study of Spy1 mediated cell cycle effects throughout the development of CNS and in response to potential malignant changes in the pools of selected NSCs.

Our *in vitro* data supports that increased levels of Spy1 in NSCs prevent functional differentiation down all lineages and enhance stemness capacity. We demonstrate that Spy1 increases proliferation while maintaining stem cell attributes of the Nestin+ population in the brains of both young and aging mice. We also show that increased levels of Spy1 in the NSCs of these mice exhibit impaired functional differentiation induced by the removal of the growth factors EGF and FGF, especially down the neuronal lineage. Our results suggest that the inhibition of neurogenesis in NTA-Spy1 mice is two-fold: 1) a decrease in the differentiation programme, and 2) an increase in symmetric cell division, both of which are holding NSCs in a stem cell state, regardless of cues. Furthermore, we see a subtle impairment in recognition memory due to an inhibition of differentiation. Our work establishes a role for Spy1 in inducing a shift in cell fate decisions that favour symmetric division over asymmetric division in NSCs and thereby maintain prolonged self-renewal, in the aging brain. A shift towards a proliferative symmetric mode of division is thought to occur due to a reduction in the length of the G1 phase, which ultimately inhibits neurogenesis and has been reported to contribute to oncogenic transformation in multiple models before [62, 63, 64].

A well-established regulatory mechanism in mode of division is the segregation of the cell fate determinant protein Numb which is negatively regulated via activity of Msi1. Moreover, Numb inhibits the Notch signaling pathway, which is critical to stem cell self-renewal and symmetric division [65]. Spy1/CDK signalling has been implicated as a conserved mechanism for activation of Msi1 in mammalian cells and during oocyte maturation [53]. Our results show that Spy1 regulates mode of division in NSCs via Msi1 and NTA-Spy1 cells downregulate classical transcriptional targets of Notch1 pathway in the face of Msi1 knockdown. Hence, Spy1/CDK2- mediated effects upstream of Msi1 may potentially be involved in memory. It is important to stress, however, that at this time we cannot draw explicit details with regards to how increased Msi1 through Spy1 changes the neural populations of cells that are involved with memory. Further work will aid in elucidating specific molecular mechanisms that could be altered in neurogenesis that also play important roles in memory as well as potentially memory-related disorders.

Msi1-Numb-Notch axis has been also implicated previously in malignant transformation [66] and our work provides evidence that Spy1 relies on this pathway to maintain pools of NSCs in he brains of NTA-Spy1 aging mice surpassing the lifespan of the NSCs in control animals. Normal brain homeostasis involves downregulation of the pools of active NSCs with increasing age by upregulation of CKIs including p16 to counteract potential oncogenic transformation [67,68]. Previously published studies showed that aging populations of NSCs accumulated dangerous changes in critical genes guarding their integrity and persistence of those changes results in tumourigenesis [68]. Spy1 can activate both CDK1 and CDK2 independently of critical phosphorylation and dephosphorylation events compared to their cyclin-binding partners [17] allowing for

overriding of the cell cycle checkpoints and cell cycle progression in non-permissive, cell protective circumstances. Spy1 can also promote the degradation of the CKI, p27 [18] and Spy1/CDK2 complex demonstrates lower sensitivity to p21- mediated inhibition [69]. Our data demonstrate that combining downregulation of tumour suppressor levels such as p53 or PTEN and/or overexpression of potent oncogenes, frequently found in brain tumours, with upregulation of Spy1 in normal NSCs increases oncogenic transformation *in vitro*. NTA-Spy1 cultures show increased viability in anchorage independent conditions and enhanced colony formation capacity. We demonstrate that Spy1 mediated changes in NSCs drive their resistance to the standard chemotherapy agent and the effect is enhanced in face of tumour suppressor downregulation and/or overexpression of an oncogene. Although further, fine-tuned, extensive analysis of pro-oncogenic changes cooperating with Spy1 to drive tumourigenesis *in vivo* is warranted we show that downregulation of Spy1 levels in mouse glioblastoma cell line with abrogated p53 and Ras protein mutation, results in decreased tumour burden upon orthotopic injection into the syngeneic mouse model.

In summary, results of our study show that upregulation of Spy1 under the Nestin promoter results in increased proliferation and expansion of symmetrically dividing NSCs in the adult mammalian brain, leading to decline of neurogenesis and increased susceptibility to malignant transformation in face of selected pro-tumourigenic changes.

Limitations of the study

In this work the expression of Spy1 is driven *in vivo* under the control of the neuroepithelial stem cell protein (Nestin) promoter. The selection of Nestin promoter allows for Spy1 to be selectively driven in the neural stem cell population. This does not

address the potential impact that Spy1 may have on cells outside of the neural stem cell population. Another limitation in our study is the use of lentiviral transduction of shRNA against Spy1 which is transient in nature and prevents long-term assessment of the effects of Spy1 depletion in our glioma syngeneic graft model. We also acknowledge that our study is limited to the effects mediated by one member of the Speedy/RINGO family of proteins, Spy1A. Other Spy1 family members are found to be elevated in human glioma, and it is possible that other family members play roles in neural stem cells and brain development. Our knockdown studies also do not address potential compensation by these family members or other cell cycle proteins. The potential of redundancy becomes particularly important when considering therapeutic translation of these findings and is worthy of future studies.

AUTHOR CONTRIBUTIONS

IQ, DL, FKS, HPM, SA, EB, AR, and MA carried out the experiments presented in this manuscript. IQ, DL, FKS, BF and LAP supported experimental design. DL, BF, JB, HPM supported derivation and maintenance of the mouse colony. IQ, DL, AR, SK supported data analysis. IQ, DL, FKS, HPM, SA, JB, BF and LAP supported the writing of this manuscript. Grant funding to LAP supported this project. All authors edited the manuscript and provided comments on the intellectual content.

ACKNOWLEDGEMENTS

We would like to thank staff in the animal care facility at the University of Windsor as well as Dr. Elizabeth Fidalgo da Silva in the Flow Cytometry Core Facility at the

University of Windsor for their support. IQ, AR and KFS acknowledge support from the Queen Elizabeth II Ontario Graduate Scholarship. EB acknowledges support from the Natural Sciences and Engineering Research Council of Canada for Undergraduate Student Research Award. This work was supported by operating funds from the Canadian Institutes Health Research to LAP (Grant #406811).

DECLARATION OF INTERESTS

We have no conflicts to claim.

Inclusion and Diversity Statement

Brain development and abnormal brain conditions including cancer, affect men and women alike and hence both male and female mice were used in this study.

FIGURE LEGENDS

Figure 1. Characterization of NTA-Spy1 transgenic mouse

(A) Schematic representation of the Nestin-rtTA transactivator mouse crossed with pTRE-Spy1 target transgenic mouse. Doxycycline addition turns on Spy1 under Nestin promoter.

(B) QRT-PCR gene expression analysis for Flag (top) and Spy1 (bottom) in wildtype (WT), Nestin-rtTA, pTRE-Spy1, and NTA-Spy1 primary neurosphere cultures without and with the addition of doxycycline (Dox).

(C) Western blot (left) for Spy1 protein using primary neurosphere cultures from pTRE-Spy1 and NTA-Spy1 littermates without and with doxycycline (Dox) addition.

Densitometry analysis, expression shown as Integrated Density Values (IDV) of Spy1/Actin in pTRE-Spy1 and NTA-Spy1 littermates.

(D) QRT-PCR gene expression levels of Spy1 in FACS sorted populations for Nestin- and Nestin+ cells from pTRE-Spy1 and NTA-Spy1 littermates. QRT-PCR values are normalized to GAPDH. Results presented as the mean ±s.d.; *$p < 0.05$, **$p < 0.01$, ***$p < 0.001$; Student's *t*-test.

Figure 2. NTA- Spy1 mice have enhanced stemness characteristics

(A) BrdU incorporation assay; representative images (left) in wildtype (WT), Nestin-rtTA, pTRE-Spy1, and NTA-Spy1 cells. BrdU+ cells scored and quantified as percentage of total population tested (right). Scale bar = 50 µm

(B) Neurosphere formation assay over three serial passages (primary- 1°, secondary- 2°, tertiary- 3°) of wildtype (WT), Nestin-rtTA, pTRE-Spy1, and NTA-Spy1 cells; representative images (left), quantified number of neurospheres (right). Scale bar = 100 µm.

(C) Neurospheres derived from wildtype (WT), Nestin-rtTA, pTRE-Spy1, and NTA-Spy1 cells measured in diameter over three serial passages (primary- 1°, secondary- 2°, tertiary- 3°).

(D) Clonal assay quantified as percentage of single cells forming spheres in pTRE-Spy1 and NTA-Spy1 cells.

(E) QRT-PCR analysis for gene expression of CD133, Nestin and Sox2 in the primary, secondary and tertiary neurospheres of NTA-Spy1 and pTRE-Spy1 cells.

(F) QRT-PCR gene expression analysis for Oct4, Sox2, Klf4, c-Myc and Nanog in NTA-Spy1 cultures relative to the expression levels in pTRE-Spy1 cells. QRT-PCR values are normalized to GAPDH. Results presented as the mean ±s.d.; *p < 0.05, **p < 0.01, ***p < 0.001; Student's *t*-test.

Figure 3. NTA-Spy1 mice have decreased differentiation capacity

(A) pTRE-Spy1 and NTA-Spy1 cells subjected to differentiation using 2% FBS. Number of differentiated cells scored and quantified as percentage of population tested at each indicated time point (right). Representative images (left). Scale bar = 30 µm.

(B) QRT-PCR analysis for astrocyte specific (S-100β), oligodendrocyte specific (O4) and neural specific (Beta III Tubulin, Mapt) genes in pTRE-Spy1 and NTA-Spy1 cells at the indicated time points of differentiation. QRT-PCR values are normalized to GAPDH.

(C) Western blot (left) for CKI and differentiation associated protein p27, in pTRE-Spy1 and NTA-Spy1 neurospheres derived from mice at the postnatal day 4. Actin was used as a loading control. Expression levels quantified using densitometry and graphed as p27/Actin ratio of Integrated Density Values (IDV) in pTRE-Spy1 and NTA-Spy1 cells. Results presented as the mean ±s.d.; *p < 0.05, **p < 0.01, ***p < 0.001; Student's *t*-test.

Figure 4. NTA-Spy1 mice show increased symmetric division through Msi1 mediated mechanism

(A) pTRE-Spy1 (left) and NTA-Spy1 (right) cultured in Matrigel™. Cells scored for differentiation and colony formation, quantified as percentage of the number of cells seeded.

(B) Cell pair assay in MaxGel ECM. Representative images of Numb protein distribution in mitotic pairs (left) of pTRE-Spy1 (top) and NTA-Spy1 (bottom). Mitotic cell pairs were scored (right) as asymmetric or symmetric and graphed as a percent of total mitotic pairs counted in pTRE-Spy1 and NTA-Spy1 cells.

(C) Schematic of Msi1 signaling.

(D) Western blot for Msi1, Numb (left). Actin used as a loading control. Densitometry analysis (right) of Musashi/Actin Integrated Density Values (IDV) and Numb/Actin IDV in pTRE-Spy1 and NTA-Spy1 cells.

(E) QRT-PCR analysis for gene expression of Msi1 (left) and Hes1 and Hes5 (right) in pTRE-Spy1 and NTA-Spy1 cells treated with siMsi1. Expression quantified as LogRQ values relative to siControl.

(F) Cell pair assay in pTRE-Spy1 and NTA-Spy1 siMsi1 cells vs. control (siControl). Results presented as the mean ±s.d.; *$p < 0.05$, **$p < 0.01$, ***$p < 0.001$; Student's *t*-test.

Figure 5. Aging NTA- Spy1 mice retain NSC pool and present with impaired cognitive functions

(A) BrdU incorporation assay; representative images of cells derived from aged (20-month old) Nestin-rtTA, pTRE-Spy1, and NTA-Spy1 mice (left). BrdU+ cells scored and quantified as percentage of total population tested (right). Scale bar = 50 µm.

(B) Cells derived from aged Nestin-rtTA, pTRE-Spy1 and NTA-Spy1 mice subjected to differentiation using 2% FBS. Number of differentiated cells scored and quantified as percentage of population tested at each indicated time point.

(C) Nestin-rtTA and NTA-Spy1 derived brain sections stained for PCNA representative images (top) and scored PCNA+ cells (bottom). Scale bar = 200 µm.

(D) QRT-PCR analysis for Ki67 in aged pTRE-Spy1 and NTA- Spy1 derived neurosphere cultures.

(E) QRT-PCR analysis for CKI genes p21, INK4 and p53 in cells derived from aged NTA-Spy1 mice. Gene expression quantified as LogRQ ratio to pTRE-Spy1.

(F) γH2A.X immunofluorescence representative imaged (left) in aged pTRE-Spy1 and NTA-Spy1 derived cells. Scale bar = 20 µm. The average number of γH2A.X foci quantified per cell (right).

(G) Caspase 3/7 activity quantified as CPS $x10^3$ units in neurosphere cultures derived from aged pTRE-Spy1 and NTA-Spy1 littermates.

(H) Analysis and quantification of the distribution of Nissl+ neuronal cells in the cortical plate using aged Nestin-rtTA and NTA-Spy1 brain sections.

(I) Schematic of novel object recognition memory test (top). Preference for novel object at day 4 measured as a percentage of time spent at novel object versus the overall time spent at objects in aged control mice (Nestin-rtTA, pTRE-Spy1) and NTA-Spy1 mice (bottom); (n=12). Results presented as the mean ±s.d.; *$p < 0.05$, **$p < 0.01$; Student's *t*-test.

Figure 6. Spy1 overexpression induces aberrant changes in characteristics of normal NSCs

(A) Immunohistochemistry- based analysis of p53 protein expression levels in cortex (CX), subventricular zone (SVZ) and, hippocampus (HC). Number of positive cells

scored and quantified over total cell number in a filed of view, over five fields of view in three separate mice, using ImageJ. DAPI was used as a nuclear counterstain.

(B). Immunohistochemistry- based analysis of Pten protein expression levels in cortex (CX), subventricular zone (SVZ) and, hippocampus (HC). Number of positive cells scored and quantified over total cell number in a filed of view, over five fields of view in three separate mice, using ImageJ. DAPI was used as a nuclear counterstain.

(C) qRT-PCR analysis of mRNA expression levels of CCND1 and c-Myc in neurosphere cultures derived from littermate pTRE-Spy1 and NTA-Spy1 mice and transduced with shp53 and/or treated with PTEN inhibitor (PTENi). Results presented as the mean ±s.d.; *$p < 0.05$, **$p < 0.01$, ***$p < 0.001$; Student's *t*-test.

Figure 7. Spy1 plays a role in oncogenic transformation of NSCs

(A) Soft agar colony formation assay in NTA-Spy1 and pTRE-Spy1 cultures transduced with shp53/sh-scrambled control and/or treated with PTENi/vehicle control. Colonies were stained with crystal violet and scored and graphed as average number of colonies.

(B) Soft agar colony formation assay in NTA-Spy1 and pTRE-Spy1 cultures transduced with RasV12/pEIZ-Control vector. Colonies were stained with crystal violet and scored and graphed as an average number of colonies.

(C) Zebrafish tumour foci formation assay using xenografted NTA-Spy1 and/or pTRE-Spy1 cells treated with si-p53 versus si-control (siCnt). Left: image panel of zebrafish xenografts at 4 days post injection. Right: foci of at least 50 microns in diameter scored per zebrafish larvae using ImageJ software.

(D) Tumour burden at day 15 in C57BL/6 mice grafted with GL261 cells transduced with pLB-scrambled control or pLB-shSpy1. Tumours imaged using SII Ami-HT *in vivo* imager and fluorescence intensity measured using Aura software and quantified as Average Radiant Efficiency over 8 mice per treatment.

(E) Caspase 3/7 activity assay in NTA-Spy1 and pTRE-Spy1 cells (left) and NTA-Spy1 cells treated with 25µM TMZ in the presence and/or absence of si-p53.

(F) Viability of NTA-Spy1 and pTRE-Spy1 cells transduced with RasV12 and treated with 30µM NU2058 and/or 25µM TMZ alone or combined, assayed using 3D Cell Titer Glo and quantified as Relative Luminescence Units (RLU). Data are shown as mean ± s.d., n=3. *$p < 0.05$, **$p < 0.01$, ***$p < 0.001$; Student's *t*-test.

STAR METHODS

RESOURCE AVAILABILITY

Lead contact

Any inquiries and requests for reagents, materials or additional information should be directed to Lisa A. Porter (lporter@uwindsor.ca).

Materials availability

Materials from this study are available upon request from the lead contact and upon signing of an MTA.

Data and code availability

All data can be obtained from the lead contact upon request. Any additional information required to reanalyze the data reported in this paper is available from the lead contact upon request. This article does not include original code.

EXPERIMENTAL MODELS AND SAMPLE DETAILS

Generation of Spy1-pTRE Transgene

Site directed mutagenesis was performed to create an Xbal site in Flag-Spy1A-pLXSN[70]. The pTRE-Tight caspase 3 (p12):n2[TU#817] plasmid (Addgene 16084) was digested with EcoRI and Xbal to remove the caspase 3. Flag-Spy1 from the Flag-Spy1A-pLXSN vector was ligated into the pTRE-Tight backbone.

Generation and Maintenance of Spy1-pTRE Mice and Maintenance of Nestin-rtTA

Animal care and use procedures follow the Canadian Council on Animal Care Guidelines under the animal utilization protocol approved by the University of Windsor (AUPP #22-09). XhoI enzyme was used to remove the Spy1-pTRE transgene fragment from the Spy1-pTRE vector. The transgenic fragment was sent to London Regional Transgenic and Gene Targeting Facility to use for pronuclear injections into B6CBAF1/J hybrid embryos. PCR analysis was used to identify founders and maintain the colony. A 25µL PCR reaction was prepared comprising of 100-150ng of genomic DNA, 0.4uM forward primer, 0.4uM reverse primer (Supplemental Table 1), and 12.5µL of New England Biolabs Master Mix. The PCR cycling conditions used are as follows: 95°C for 2 minutes and 30 seconds; 95°C for 30 seconds, 60°C for 45 seconds and 72°C for 1 minute and 30 seconds (40 cycles); this was followed by a final extension at 72°C for 10 minutes.

Nestin-rtTA mice were purchased from the Jackson Laboratory [FVB/N-Tg (Nes-rtTA) 306Rsv/J] or from in house breeding at the University of Windsor. Genotyping was performed using 25µL PCR reactions containing 1 µL of genomic DNA, 0.4uM forward primer, 0.4uM reverse primer (Supplemental Table 1), and 12.5µL of New England Biolabs Master Mix. The PCR cycling conditions used are as follows: 94°C for 3

minutes; 94°C for 30 seconds, 57°C for 1 minute and 72°C for 1 minute (35 cycles); this was followed by a final extension at 72°C for 2 minutes.

METHOD DETAILS

Primary Neural Stem Cell Isolations and Cell Culture

Mice were humanely euthanized, and a midline incision was made to the skin along the full length of mouse. The skull was cut at the sides and peeled off with forceps. Cranial nerves and blood vessels were cut, and forceps were used to extract the brain. The brain was transferred to a 60mm dish containing media with 3% penicillin/streptomycin (P/S) solution, sliced coronally and the area around the lateral ventricles was dissected under a microscope. Tissue was transferred to a separate dish with 3% P/S solution and, using a scalpel blade, tissue was minced and collected by centrifugation. The supernatant was removed and 1 ml of Trypsin- 0.05% EDTA (Thermo) added. The cells were incubated for 1 minute at 37°C, 1 ml of media containing 10% fetal bovine serum (FBS) was added and incubated for 5 minutes and cells were collected.

Primary cells were cultured as neurospheres in serum-free Neurobasal medium (Corning) containing B27 supplement (Gibco), hEGF (20ng/ml; Gibco) and bFGF (10ng/ml; Sigma), 2 mM L-glutamine at 37°C in 5% CO_2 in ultra-low cluster plates (ULCP; Corning). Neurospheres were subcultured every 5-10 days. Neurosphere formation assays were conducted in 6-well ULCP plates at a density of 50,000 cells per well. Clonal assays were performed in neurosphere media in 96-well ULCP plates. Cells were plated through serial dilution and wells containing 1-5 cells were included for experimental analysis.

For differentiation experiments, single cells were dissociated from primary neurospheres and seeded in media supplemented with 2% FBS (Gibco) as previously described[38]. For all lineage specific differentiation protocols, single cells were seeded in polyornithine (Sigma) coated plates and supplemented with different growth mediums. For neuronal-specific differentiation, cells were given Neurobasal medium (Corning) supplemented with 2% B27 (Gibco) and 2 mM GlutaMAX-I (Gibco) for 7 days to which dibutyryl cAMP (Sigma) was added to a final concentration of 0.5mM for 3 days. For astrocyte differentiation, single cells were seeded in DMEM (Thermo) supplemented with 1% N2 (Thermo), 2mM GlutaMAX-I (Gibco), and 1% FBS for 7 days with media changes every other day. For oligodendrocyte-specific differentiation, single cells were seeded in Neurobasal medium (Corning) supplemented with 2% B27 (Gibco), 2mM GlutaMAX-I (Gibco) and 30 ng/mL T3 (Sigma) for 7 days with media changes every other day.

Orthotopic Cell Transplantation into Mice

C57BL/6 neonatal mice at postnatal day 1 were cryoanaesthetized and transplanted with 25000 GL261 cells orthotopically into the brain using a stereotactic injector (Stoelting co.) coordinated using Neurostar software coordinating the injection site from bregma as the 0 point to X, Y, Z = (0.8, 2.0, -1.5mm). The cells were injected in 2ul at the rate of 30nl per min.

Quantitative Real Time-PCR (qRT-PCR) Analysis

Total RNA was isolated using Qiagen RNeasy Plus Mini Kit as per manufacturer's instructions. cDNA was synthesized using qSCRIPT (Quanta) as per manufacturer's

instructions. Reactions were prepared using Fast SYBR Green master mix and run/analyzed using Viia7 qRT-PCR System (Life Technologies) and software. Changes to mRNA expression levels were presented as Relative Quantification (RQ) values or $\log_{10}$ RQ. Primer sequences are collected in supplementary material Table 1.

Bromodeoxyuridine (BrdU) Proliferation Assay

Cells were incubated in media containing BrdU (BD Pharmingen) at a concentration of 10 µM overnight at 37°C, 5% CO_2. Cells were fixed in 4% PFA and incubated with 2M HCl for 20 minutes at 37°C and subsequently incubated with Anti-BrdU (BD Biosciences) in 0.1% Tween/PBS for 45 minutes at room temperature. Cells were incubated with Alexa-568 anti-mouse (Invitrogen) for 1 hour at room temperature. This was followed by Hoechst (Thermo) counterstain for 10 minutes at room temperature. Cells were imaged using the Leica CTR 6500 microscope (Leica Microsystems, Heidelberg, Germany).

Beta-galactosidase (β-gal) Stain

Cells were fixed in 4% PFA for 10 minutes at room temperature. Staining solution (5mM $K_4[Fe(CN)_6]\cdot 3\ H_2O$, 5 mM $K_3[Fe(CN)_6]$ and 2 mM $MgCl_2$) was prepared in 1X PBS. Complete staining solution was prepared right before staining and contained 25µL of 40mg/mL X-gal per mL of staining solution. Cells were stained overnight at 37°C. Cells were imaged using the Leica CTR 6500 microscope (Leica Microsystems, Heidelberg, Germany).

Immunocytochemistry

Cells were washed with PBS and fixed in 4% PFA for 10 minutes at room temperature. Cells were permeabilized using 0.2% triton-X in 1X PBS for 10 minutes at room temperature and blocked using 10% normal goat serum. Cells were incubated with primary antibody (γH2A.X; Millipore) for 1 hour at room temperature. Cells were incubated with secondary Alexa-fluor anti-mouse (Thermo) for 45 minutes at room temperature. Finally, cells were counterstained with Hoechst (Thermo) for 10 minutes at room temperature. Coverslips were mounted on slides and imaged using the Leica CTR 6500 microscope (Leica Microsystems, Heidelberg, Germany).

Protein Isolation and Immunoblotting

Cells were lysed with TNE buffer for 20 minutes (50mM Tris, 150mM NaCl, 5mM EDTA) and supplemented with protease inhibitors (2µg/mL leupeptin, 5µg/mL aprotinin, and 100µg/mL PMSF). Cells were centrifuged at 4°C at 13,000rpm for 15 minutes and the supernatant was collected. Protein concentrations were determined through the Bradford assay as per manufacturer's instructions.

100µg of protein were loaded on a 10%- SDS polyacrylamide gel and ran for 3 hours at 120V. The gels were transferred to a PVDF membrane at 30V for 2 hours using a wet transfer method. Membranes were blocked for 1 hour at room temperature in either 2% BSA or 2% milk, depending on antibodies used. Primary antibodies were incubated overnight at 4°C. Following incubation with primary antibody, membranes were washed with tris-buffered-saline-tween 20 (TBST) 3 times for 8 minutes each. This was followed with secondary antibody incubation at room temperature for 1 hour. Following secondary antibody incubation, membranes were washed 3 times in TBST for 5-minute intervals. Protein signal was detected using chemiluminescent peroxidase substrate (Pierce) as per

manufacturer's instructions. Images were taken on Alpha Innotech HD2, densitometry and analysis were performed on AlphaEase FC software.

Antibodies

For immunoblot analysis, antibodies used include: Actin (Millipore, 1:1000), Spy1 (Abcam, 1:700), Sox2 (Cell Signaling, 1:1000), Klf4 (R&D Systems; 1:800), p27 (Abcam, 1:800), Musashi 1 (Abcam, 1:1000), and Numb (Abcam, 1:800). All secondary antibodies, mouse IgG (Sigma Aldrich) and rabbit IgG (Sigma Aldrich), were used at a concentration of 1:10,000.

Immunofluorescent Cell Pair Assay

Single cells were isolated with 0.05% Trypsin-EDTA and plated in a drop of media onto MaxGel™ ECM (Sigma) coated coverslips. Cell division was monitored over 20 hours and then fixed in 4% PFA for 15 minutes at room temperature. Cells were washed, permeabilized and incubated with 1:200 Numb antibody (Cell signaling). Alexa-fluorophore conjugated secondary antibody (1:1000 dilution) (Invitrogen) was applied for 30 minutes. TOTO-3 was used as a nuclear counterstain. Five random fields of view were scored for Numb protein distribution in mitotic cell pairs/treatment/replicate. Analysis was performed using Leica CTR 6500 microscope (Leica Microsystems, Heidelberg, Germany) and AF software.

Novel Object Recognition Test

Novel object recognition test was performed as described [71]. Plexiglass boxes were built with the dimensions of 40cm x 40cm x 40cm and covered with frosted white paper to impair outside views from the box. Plastic cubes were used as objects and were

approximately 4cm x 4cm x 4cm. The objects were either blue or yellow in colour. Computer cameras were used to record the videos. On days 1 and 2, mice were moved to an area near the boxes for 10 minutes. To acclimate the mice to their environment and decrease stress, the mice were then individually placed directly in the boxes for 10 minutes on both days. Plexiglass boxes and the objects were cleaned with 70% ethanol after every mouse and dried for 10 minutes before the next mouse was placed inside. On day 3, mice were transported to an area near boxes and allowed to sit in holding cages for 10 minutes. Similarly, mice were then placed in the boxes to explore for 10 minutes and were recorded. Day 4 was testing day, where one of the old objects was replaced with a novel object. Similarly, mice were taken to an area near the boxes, allowed to sit for 10 minutes, and then placed inside the boxes and recorded for 10 minutes. The exploration time was counted by the period that the mice stayed facing the object within a 5 cm radius of the object. Exploration times of under 20 seconds or over 5 minutes at an object were excluded. Preference rate was measured by dividing the total time spent exploring both objects by the time spent exploring one object.

STATISICAL ANALYSIS

Student's *t*-test was used and a p-value of less than 0.05 was considered significant. All data are reported as a means of standard deviation. For qRT-PCR analysis, cycle threshold (Ct) values of internal control gene (GAPDH) were subtracted from the corresponding Ct value of a target gene which generated a ΔCt value which was subjected to the Student *t*-test analysis. For comparative analysis between (WT), Nestin-rtTA, pTRE-Spy1, and NTA-Spy1mice and primary cultures, littermate mice were used.

REFERENCES

1. Alvarez-Buylla, A., and Lim, D.A. (2004). For the long run: maintaining germinal niches in the adult brain. Neuron *41*, 683–686. 10.1016/s0896-6273(04)00111-4.

2. Lie, D.C., Song, H., Colamarino, S.A., Ming, G., and Gage, F.H. (2004). Neurogenesis in the Adult Brain: New Strategies for Central Nervous System Diseases. Annu. Rev. Pharmacol. Toxicol. *44*, 399–421. 10.1146/annurev.pharmtox.44.101802.121631.

3. Lois, C., and Alvarez-Buylla, A. (1994). Long-Distance Neuronal Migration in the Adult Mammalian Brain. Science *264*, 1145–1148. 10.1126/science.8178174.

4. Park, D., Xiang, A.P., Mao, F.F., Zhang, L., Di, C.-G., Liu, X.-M., Shao, Y., Ma, B.-F., Lee, J.-H., Ha, K.-S., et al. (2010). Nestin is required for the proper self-renewal of neural stem cells. Stem Cells Dayt. Ohio *28*, 2162–2171. 10.1002/stem.541.

5. Namiki, J., Suzuki, S., Masuda, T., Ishihama, Y., and Okano, H. (2012). Nestin protein is phosphorylated in adult neural stem/progenitor cells and not endothelial progenitor cells. Stem Cells Int. *2012*, 430138. 10.1155/2012/430138.

6. Urbán, N., Blomfield, I.M., and Guillemot, F. (2019). Quiescence of Adult Mammalian Neural Stem Cells: A Highly Regulated Rest. Neuron *104*, 834–848. 10.1016/j.neuron.2019.09.026.

7. Liu, L., Michowski, W., Kolodziejczyk, A., and Sicinski, P. (2019). The cell cycle in stem cell proliferation, pluripotency and differentiation. Nat. Cell Biol. *21*, 1060–1067. 10.1038/s41556-019-0384-4.

8. Salomoni, P., and Calegari, F. (2010). Cell cycle control of mammalian neural stem cells: putting a speed limit on G1. Trends Cell Biol. *20*, 233–243. 10.1016/j.tcb.2010.01.006.

9. Neumüller, R.A., and Knoblich, J.A. (2009). Dividing cellular asymmetry: asymmetric cell division and its implications for stem cells and cancer. Genes Dev. *23*, 2675–2699. 10.1101/gad.1850809.

10. Ghatak, D., Das Ghosh, D., and Roychoudhury, S. (2021). Cancer Stemness: p53 at the Wheel. Front. Oncol. *10*, 604124. 10.3389/fonc.2020.604124.

11. Tsukada, T., Tomooka, Y., Takai, S., Ueda, Y., Nishikawa, S., Yagi, T., Tokunaga, T., Takeda, N., Suda, Y., and Abe, S. (1993). Enhanced proliferative potential in culture of cells from p53-deficient mice. Oncogene *8*, 3313–3322.

12. Meletis, K., Wirta, V., Hede, S.-M., Nistér, M., Lundeberg, J., and Frisén, J. (2006). p53 suppresses the self-renewal of adult neural stem cells. Development *133*, 363–369. 10.1242/dev.02208.

13. Marin Navarro, A., Pronk, R.J., van der Geest, A.T., Oliynyk, G., Nordgren, A., Arsenian-Henriksson, M., Falk, A., and Wilhelm, M. (2020). p53 controls genomic stability and temporal differentiation of human neural stem cells and affects neural

organization in human brain organoids. Cell Death Dis. *11*, 1–16. 10.1038/s41419-019-2208-7.

14. Galvao, R.P., Kasina, A., McNeill, R.S., Harbin, J.E., Foreman, O., Verhaak, R.G.W., Nishiyama, A., Miller, C.R., and Zong, H. (2014). Transformation of quiescent adult oligodendrocyte precursor cells into malignant glioma through a multistep reactivation process. Proc. Natl. Acad. Sci. U. S. A. *111*, E4214–E4223. 10.1073/pnas.1414389111.

15. Sviderskiy, V.O., Blumenberg, L., Gorodetsky, E., Karakousi, T.R., Hirsh, N., Alvarez, S.W., Terzi, E.M., Kaparos, E., Whiten, G.C., Ssebyala, S., et al. (2020). Hyperactive CDK2 Activity in Basal-like Breast Cancer Imposes a Genome Integrity Liability that Can Be Exploited by Targeting DNA Polymerase ε. Mol. Cell *80*, 682-698.e7. 10.1016/j.molcel.2020.10.016.

16. Mahmnoudian, E., Qu, D., Lotfipour, F., and Jahani-Asl, A. (2023). TARGETING CANCER STEM CELLS WITH A CDK2 INHIBITOR IN GLIOBLASTOMA. Neuro-Oncol. Adv. *5*, i11. 10.1093/noajnl/vdad071.049.

17. Cheng, A., Xiong, W., Ferrell, Jr., James E., and Solomon, M.J. (2005). Identification and Comparative Analysis of Multiple Mammalian Speedy/Ringo Proteins. Cell Cycle *4*, 155–165. 10.4161/cc.4.1.1347.

18. McGrath, D.A., Fifield, B.-A., Marceau, A.H., Tripathi, S., Porter, L.A., and Rubin, S.M. (2017). Structural basis of divergent cyclin-dependent kinase activation by Spy1/RINGO proteins. EMBO J. *36*, 2251–2262. 10.15252/embj.201796905.

19. Lenormand, J.-L., Dellinger, R.W., Knudsen, K.E., Subramani, S., and Donoghue, D.J. (1999). Speedy: a novel cell cycle regulator of the G2/M transition. EMBO J. *18*, 1869–1877. 10.1093/emboj/18.7.1869.

20. McAndrew, C.W., Gastwirt, R.F., Meyer, A.N., Porter, L.A., and Donoghue, D.J. (2007). Spy1 Enhances Phosphorylation and Degradation of the Cell Cycle Inhibitor p27. Cell Cycle *6*, 1937–1945. 10.4161/cc.6.15.4520.

21. Lubanska, D., Qemo, I., Byrne, M., Matthews, K.N., Fifield, B.-A., Brown, J., da Silva, E.F., and Porter, L.A. (2021). The cyclin-like protein SPY1 overrides reprogramming induced senescence through EZH2 mediated H3K27me3. Stem Cells Dayt. Ohio *39*, 1688–1700. 10.1002/stem.3453.

22. Gonzalez, L., Domingo-Muelas, A., Duart-Abadia, P., Nuñez, M., Mikolcevic, P., Llonch, E., Cubillos-Rojas, M., Cánovas, B., Forrow, S.M.A., Morante-Redolat, J.M., et al. (2023). The atypical CDK activator RingoA/Spy1 regulates exit from quiescence in neural stem cells. iScience *26*, 106202. 10.1016/j.isci.2023.106202.

23. Golipour, A., Myers, D., Seagroves, T., Murphy, D., Evan, G.I., Donoghue, D.J., Moorehead, R.A., and Porter, L.A. (2008). The Spy1/RINGO Family Represents a Novel

Mechanism Regulating Mammary Growth and Tumorigenesis. Cancer Res. *68*, 3591–3600. 10.1158/0008-5472.CAN-07-6453.

24. Huang, Y., Liu, Y., Chen, Y., Yu, X., Yang, J., Lu, M., Lu, Q., Ke, Q., Shen, A., and Yan, M. (2009). Peripheral Nerve Lesion Induces an Up-regulation of Spy1 in Rat Spinal Cord. Cell. Mol. Neurobiol. *29*, 403–411. 10.1007/s10571-008-9332-8.

25. Fifield, B.-A., Qemo, I., Kirou, E., Cardiff, R.D., and Porter, L.A. (2019). The atypical cyclin-like protein Spy1 overrides p53-mediated tumour suppression and promotes susceptibility to breast tumourigenesis. Breast Cancer Res. BCR *21*, 140. 10.1186/s13058-019-1211-3.

26. Fifield, B.-A., Talia, J., Stoyanovich, C., Elliott, M.J., Bakht, M.K., Basilious, A., Samsoondar, J.P., Curtis, M., Stringer, K.F., and Porter, L.A. (2020). Cyclin-like proteins tip regenerative balance in the liver to favour cancer formation. Carcinogenesis *41*, 850–862. 10.1093/carcin/bgz164.

27. Lubanska, D., and Porter, L.A. (2014). The atypical cell cycle regulator Spy1 suppresses differentiation of the neuroblastoma stem cell population. Oncoscience *1*, 336–348. 10.18632/oncoscience.36.

28. Lubanska, D., Market-Velker, B.A., deCarvalho, A.C., Mikkelsen, T., Fidalgo da Silva, E., and Porter, L.A. (2014). The Cyclin-like Protein Spy1 Regulates Growth and Division Characteristics of the CD133+ Population in Human Glioma. Cancer Cell *25*, 64–76. 10.1016/j.ccr.2013.12.006.

29. Fifield, B.-A., Qemo, I., Kirou, E., Cardiff, R.D., and Porter, L.A. (2019). The atypical cyclin-like protein Spy1 overrides p53-mediated tumour suppression and promotes susceptibility to breast tumourigenesis. Breast Cancer Res. *21*, 140. 10.1186/s13058-019-1211-3.

30. Gil-Perotin, S., Marin-Husstege, M., Li, J., Soriano-Navarro, M., Zindy, F., Roussel, M.F., Garcia-Verdugo, J.-M., and Casaccia-Bonnefil, P. (2006). Loss of p53 Induces Changes in the Behavior of Subventricular Zone Cells: Implication for the Genesis of Glial Tumors. J. Neurosci. *26*, 1107–1116. 10.1523/JNEUROSCI.3970-05.2006.

31. Gunther, E.J., Belka, G.K., Wertheim, G.B.W., Wang, J., Hartman, J.L., Boxer, R.B., and Chodosh, L.A. (2002). A novel doxycycline-inducible system for the transgenic analysis of mammary gland biology. FASEB J. *16*, 283–292. 10.1096/fj.01-0551com.

32. Hendrickson, M.L., Rao, A.J., Demerdash, O.N.A., and Kalil, R.E. (2011). Expression of Nestin by Neural Cells in the Adult Rat and Human Brain. PLOS ONE *6*, e18535. 10.1371/journal.pone.0018535.

33. Reynolds, B.A., and Weiss, S. (1992). Generation of neurons and astrocytes from isolated cells of the adult mammalian central nervous system. Science *255*, 1707–1710. 10.1126/science.1553558.

34. Reynolds, B.A., and Weiss, S. (1996). Clonal and Population Analyses Demonstrate That an EGF-Responsive Mammalian Embryonic CNS Precursor Is a Stem Cell. Dev. Biol. *175*, 1–13. 10.1006/dbio.1996.0090.

35. Takahashi, K., and Yamanaka, S. (2006). Induction of pluripotent stem cells from mouse embryonic and adult fibroblast cultures by defined factors. Cell *126*, 663–676. 10.1016/j.cell.2006.07.024.

36. Yu, J., Vodyanik, M.A., Smuga-Otto, K., Antosiewicz-Bourget, J., Frane, J.L., Tian, S., Nie, J., Jonsdottir, G.A., Ruotti, V., Stewart, R., et al. (2007). Induced Pluripotent Stem Cell Lines Derived from Human Somatic Cells. Science *318*, 1917–1920. 10.1126/science.1151526.

37. Suvà, M.L., Rheinbay, E., Gillespie, S.M., Patel, A.P., Wakimoto, H., Rabkin, S.D., Riggi, N., Chi, A.S., Cahill, D.P., Nahed, B.V., et al. (2014). Reconstructing and reprogramming the tumor-propagating potential of glioblastoma stem-like cells. Cell *157*, 580–594. 10.1016/j.cell.2014.02.030.

38. Kerosuo, L., Piltti, K., Fox, H., Angers-Loustau, A., Häyry, V., Eilers, M., Sariola, H., and Wartiovaara, K. (2008). Myc increases self-renewal in neural progenitor cells through Miz-1. J. Cell Sci. *121*, 3941–3950. 10.1242/jcs.024802.

39. Bahrami, A.R., Matin, M.M., and Andrews, P.W. (2005). The CDK inhibitor p27 enhances neural differentiation in pluripotent NTERA2 human EC cells, but does not permit differentiation of 2102Ep nullipotent human EC cells. Mech. Dev. *122*, 1034–1042. 10.1016/j.mod.2005.04.011.

40. Zheng, Y.-L., Li, B.-S., Rudrabhatla, P., Shukla, V., Amin, N.D., Maric, D., Kesavapany, S., Kanungo, J., Pareek, T.K., Takahashi, S., et al. (2010). Phosphorylation of p27Kip1 at Thr187 by Cyclin-dependent Kinase 5 Modulates Neural Stem Cell Differentiation. Mol. Biol. Cell *21*, 3601–3614. 10.1091/mbc.e10-01-0054.

41. McAndrew, C.W., Gastwirt, R.F., Meyer, A.N., Porter, L.A., and Donoghue, D.J. (2007). Spy1 enhances phosphorylation and degradation of the cell cycle inhibitor p27. Cell Cycle Georget. Tex *6*, 1937–1945. 10.4161/cc.6.15.4520.

42. Al Sorkhy, M., Fifield, B.-A., Myers, D., and Porter, L.A. (2016). Direct interactions with both p27 and Cdk2 regulate Spy1-mediated proliferation in vivo and in vitro. Cell Cycle Georget. Tex *15*, 128–136. 10.1080/15384101.2015.1121327.

44. Bertrand, V., and Hobert, O. (2009). Linking Asymmetric Cell Division to the Terminal Differentiation Program of Postmitotic Neurons in C. elegans. Dev. Cell *16*, 563–575. 10.1016/j.devcel.2009.02.011.

45. Rhyu, M.S., Jan, L.Y., and Jan, Y.N. (1994). Asymmetric distribution of numb protein during division of the sensory organ precursor cell confers distinct fates to daughter cells. Cell *76*, 477–491. 10.1016/0092-8674(94)90112-0.

46. Knoblich, J.A., Jan, and Nung Jan, Y. (1995). Asymmetric segregation of Numb and Prospero during cell division. Nature *377*, 624–627. 10.1038/377624a0.

47. Spana, E.P., Kopczynski, C., Goodman, C.S., and Doe, C.Q. (1995). Asymmetric localization of numb autonomously determines sibling neuron identity in the Drosophila CNS. Development *121*, 3489–3494. 10.1242/dev.121.11.3489.

48. Shen, Q., Zhong, W., Jan, Y.N., and Temple, S. (2002). Asymmetric Numb distribution is critical for asymmetric cell division of mouse cerebral cortical stem cells and neuroblasts. Development *129*, 4843–4853. 10.1242/dev.129.20.4843.

49. Chojnacki, A., Shimazaki, T., Gregg, C., Weinmaster, G., and Weiss, S. (2003). Glycoprotein 130 Signaling Regulates Notch1Expression and Activation in the Self-Renewal of Mammalian Forebrain Neural Stem Cells. J. Neurosci. *23*, 1730–1741. 10.1523/JNEUROSCI.23-05-01730.2003.

50. Hitoshi, S., Alexson, T., Tropepe, V., Donoviel, D., Elia, A.J., Nye, J.S., Conlon, R.A., Mak, T.W., Bernstein, A., and van der Kooy, D. (2002). Notch pathway molecules are essential for the maintenance, but not the generation, of mammalian neural stem cells. Genes Dev. *16*, 846–858. 10.1101/gad.975202.

51. Nyfeler, Y., Kirch, R.D., Mantei, N., Leone, D.P., Radtke, F., Suter, U., and Taylor, V. (2005). Jagged1 signals in the postnatal subventricular zone are required for neural stem cell self-renewal. EMBO J. *24*, 3504–3515. 10.1038/sj.emboj.7600816.

52. Okano, H., Imai, T., and Okabe, M. (2002). Musashi: a translational regulator of cell fate. J. Cell Sci. *115*, 1355–1359. 10.1242/jcs.115.7.1355.

53. Arumugam, K., MacNicol, M.C., Wang, Y., Cragle, C.E., Tackett, A.J., Hardy, L.L., and MacNicol, A.M. (2012). Ringo/Cyclin-dependent Kinase and Mitogen-activated Protein Kinase Signaling Pathways Regulate the Activity of the Cell Fate Determinant Musashi to Promote Cell Cycle Re-entry in Xenopus Oocytes*. J. Biol. Chem. *287*, 10639–10649. 10.1074/jbc.M111.300681.

54. Hovest, M.G., Brüggenolte, N., Hosseini, K.S., Krieg, T., and Herrmann, G. (2006). Senescence of human fibroblasts after psoralen photoactivation is mediated by ATR kinase and persistent DNA damage foci at telomeres. Mol. Biol. Cell *17*, 1758–1767. 10.1091/mbc.e05-08-0701.

55. Sedelnikova, O.A., Horikawa, I., Zimonjic, D.B., Popescu, N.C., Bonner, W.M., and Barrett, J.C. (2004). Senescing human cells and ageing mice accumulate DNA lesions with unrepairable double-strand breaks. Nat. Cell Biol. *6*, 168–170. 10.1038/ncb1095.

56. Narita, M., Nũnez, S., Heard, E., Narita, M., Lin, A.W., Hearn, S.A., Spector, D.L., Hannon, G.J., and Lowe, S.W. (2003). Rb-mediated heterochromatin formation and silencing of E2F target genes during cellular senescence. Cell *113*, 703–716. 10.1016/s0092-8674(03)00401-x.

57. Rotem, A., Janzer, A., Izar, B., Ji, Z., Doench, J.G., Garraway, L.A., and Struhl, K. (2015). Alternative to the soft-agar assay that permits high-throughput drug and genetic screens for cellular transformation. Proc. Natl. Acad. Sci. U. S. A. *112*, 5708–5713. 10.1073/pnas.1505979112.

58. Gastwirt, R.F., Slavin, D.A., McAndrew, C.W., and Donoghue, D.J. (2006). Spy1 expression prevents normal cellular responses to DNA damage: inhibition of apoptosis and checkpoint activation. J. Biol. Chem. *281*, 35425–35435. 10.1074/jbc.M604720200.

59. Barnes, E.A., Porter, L.A., Lenormand, J.-L., Dellinger, R.W., and Donoghue, D.J. (2003). Human Spy1 Promotes Survival of Mammalian Cells following DNA Damage1. Cancer Res. *63*, 3701–3707.

60. McAndrew, C.W., Gastwirt, R.F., and Donoghue, D.J. (2009). The atypical CDK activator Spy1 regulates the intrinsic DNA damage response and is dependent upon p53 to inhibit apoptosis. Cell Cycle *8*, 66–75. 10.4161/cc.8.1.7451.

61. Lange, C., and Calegari, F. (2010). Cdks and cyclins link G1 length and differentiation of embryonic, neural and hematopoietic stem cells. Cell Cycle Georget. Tex *9*, 1893–1900. 10.4161/cc.9.10.11598.

62. Pilaz, L.-J., Patti, D., Marcy, G., Ollier, E., Pfister, S., Douglas, R.J., Betizeau, M., Gautier, E., Cortay, V., Doerflinger, N., et al. (2009). Forced G1-phase reduction alters mode of division, neuron number, and laminar phenotype in the cerebral cortex. Proc. Natl. Acad. Sci. U. S. A. *106*, 21924–21929. 10.1073/pnas.0909894106.

63. Wang, J., Zhu, H.H., Chu, M., Liu, Y., Zhang, C., Liu, G., Yang, X., Yang, R., and Gao, W.-Q. (2014). Symmetrical and asymmetrical division analysis provides evidence for a hierarchy of prostate epithelial cell lineages. Nat. Commun. *5*, 4758. 10.1038/ncomms5758.

64. Lim, H.Y.G., and Barker, N. (2023). Sox9, A Key Regulator of Gastric Stem Cell Behavior Driving Cancer Initiation. Gastroenterology *164*, 1052–1053. 10.1053/j.gastro.2023.03.215.

65. Song, Y., and Lu, B. (2012). Interaction of Notch signaling modulator Numb with α-Adaptin regulates endocytosis of Notch pathway components and cell fate determination of neural stem cells. J. Biol. Chem. *287*, 17716–17728. 10.1074/jbc.M112.360719.

66. Forouzanfar, M., Lachinani, L., Dormiani, K., Nasr-Esfahani, M.H., Gure, A.O., and Ghaedi, K. (2020). Intracellular functions of RNA-binding protein, Musashi1, in stem and cancer cells. Stem Cell Res. Ther. *11*, 193. 10.1186/s13287-020-01703-w.

67. Kase, Y., Shimazaki, T., and Okano, H. (2020). Current understanding of adult neurogenesis in the mammalian brain: how does adult neurogenesis decrease with age? Inflamm. Regen. *40*, 10. 10.1186/s41232-020-00122-x.

68. Talma, N., Gerrits, E., Wang, B., Eggen, B.J.L., and Demaria, M. (2021). Identification of distinct and age□dependent p16High microglia subtypes. Aging Cell *20*, e13450. 10.1111/acel.13450.

69. Karaiskou, A., Perez, L.H., Ferby, I., Ozon, R., Jessus, C., and Nebreda, A.R. (2001). Differential regulation of Cdc2 and Cdk2 by RINGO and cyclins. J. Biol. Chem. *276*, 36028–36034. 10.1074/jbc.M104722200.

70. Porter, L.A., Kong-Beltran, M., and Donoghue, D.J. (2003). Spy1 Interacts with p27Kip1 to Allow G1/S Progression. Mol. Biol. Cell *14*, 3664–3674. 10.1091/mbc.e02-12-0820.

71. Huang, T.-N., and Hsueh, Y.-P. (2014). Novel Object Recognition for Studying Memory in Mice. BIO-Protoc. *4*. 10.21769/BioProtoc.1249.

Figure 1

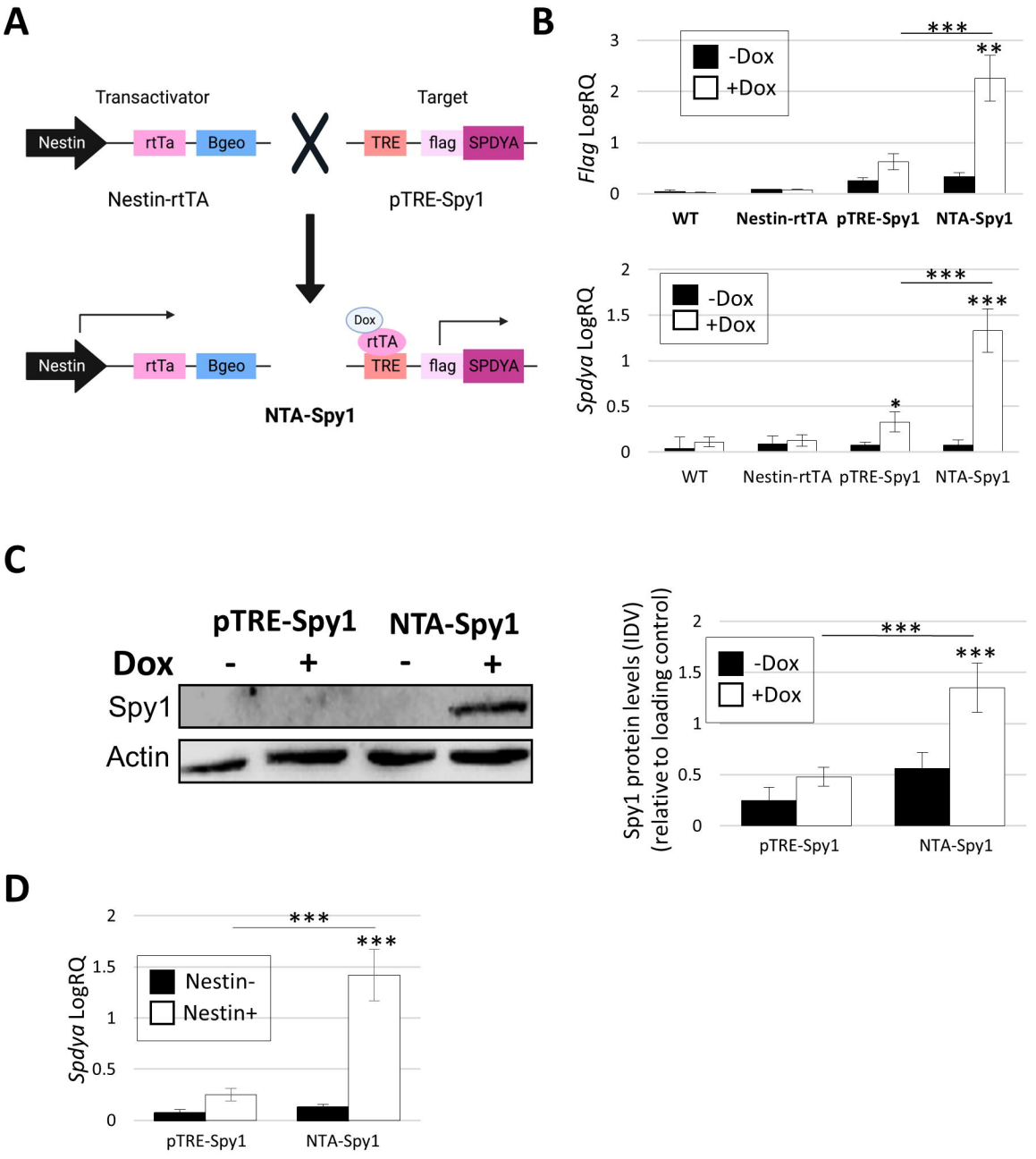
A
Transactivator
Target
Nestin
rtTa
Bgeo
TRE
flag
SPDYA
Nestin-rtTA
pTRE-Spy1
Dox
rtTA
NTA-Spy1
B
Flag LogRQ
-Dox
+Dox
***
**
WT
Nestin-rtTA
pTRE-Spy1
NTA-Spy1
Spdya LogRQ
*
C
pTRE-Spy1
NTA-Spy1
Dox
Spy1
Actin
Spy1 protein levels (IDV)
(relative to loading control)
D
Nestin-
Nestin+

Figure 2

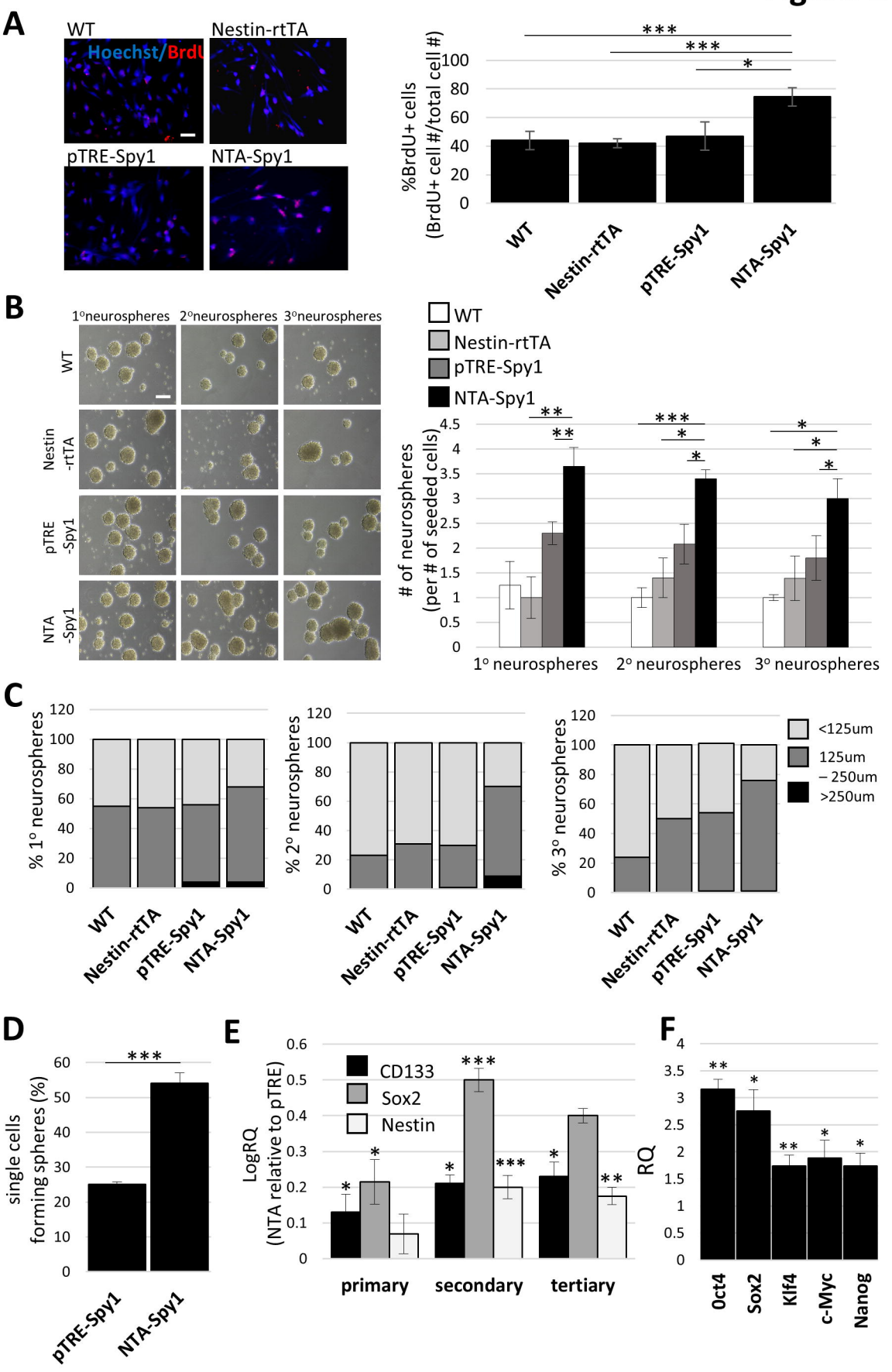
A
WT
Nestin-rtTA
Hoechst/BrdU
pTRE-Spy1
NTA-Spy1
%BrdU+ cells
(BrdU+ cell #/total cell #)
WT
Nestin-rtTA
pTRE-Spy1
NTA-Spy1
B
1°neurospheres
2°neurospheres
3°neurospheres
WT
Nestin -rtTA
pTRE -Spy1
NTA -Spy1
# of neurospheres
(per # of seeded cells)
1° neurospheres
2° neurospheres
3° neurospheres
C
% 1° neurospheres
% 2° neurospheres
% 3° neurospheres
<125um
125um – 250um
>250um
D
single cells forming spheres (%)
pTRE-Spy1
NTA-Spy1
E
LogRQ
(NTA relative to pTRE)
CD133
Sox2
Nestin
primary
secondary
tertiary
F
RQ
Oct4
Sox2
Klf4
c-Myc
Nanog

Figure 3

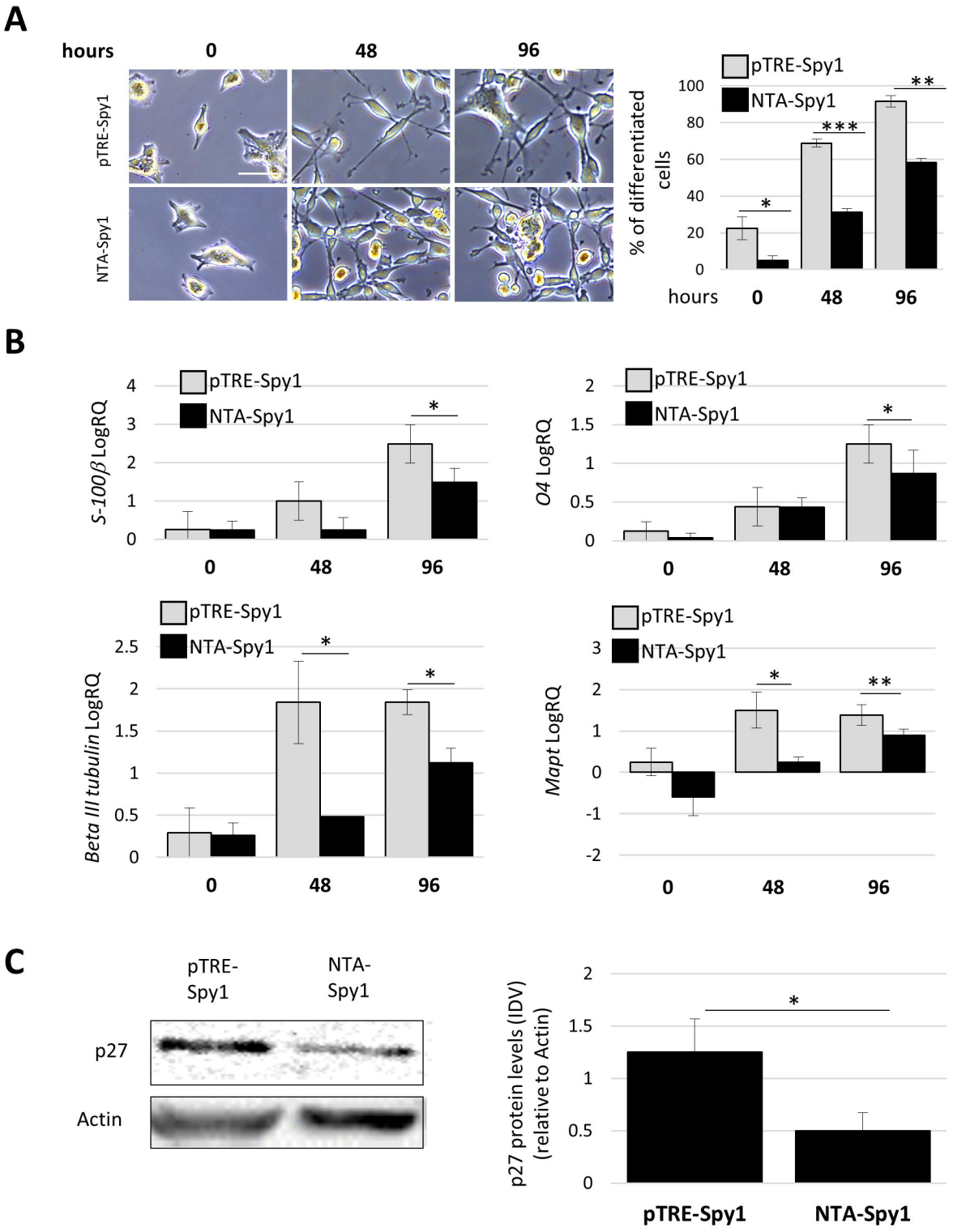
A
hours
0
48
96
pTRE-Spy1
NTA-Spy1
% of differentiated cells
100
80
60
40
20
0
*
***
**
hours
B
S-100β LogRQ
O4 LogRQ
Beta III tubulin LogRQ
Mapt LogRQ
C
pTRE-Spy1
NTA-Spy1
p27
Actin
p27 protein levels (IDV) (relative to Actin)

Figure 4

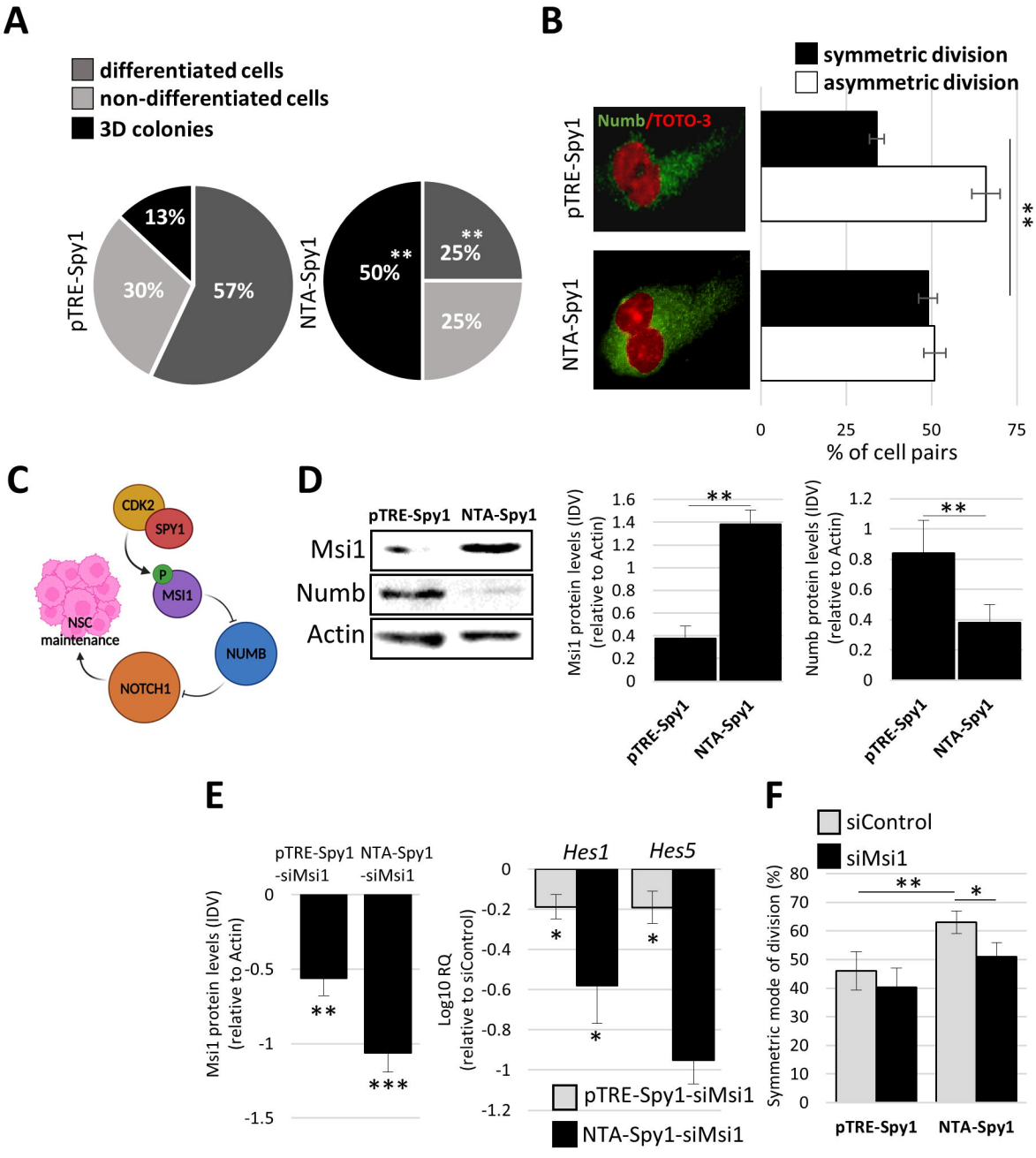
A
differentiated cells
non-differentiated cells
3D colonies
pTRE-Spy1
13%
30%
57%
NTA-Spy1
**
50%
**
25%
25%
B
symmetric division
asymmetric division
pTRE-Spy1
Numb/TOTO-3
NTA-Spy1
**
0
25
50
75
% of cell pairs
C
CDK2
SPY1
P
MSI1
NUMB
NOTCH1
NSC
maintenance
D
pTRE-Spy1
NTA-Spy1
Msi1
Numb
Actin
Msi1 protein levels (IDV)
(relative to Actin)
1.6
1.4
1.2
1
0.8
0.6
0.4
0.2
0
**
pTRE-Spy1
NTA-Spy1
Numb protein levels (IDV)
(relative to Actin)
1.2
1
0.8
0.6
0.4
0.2
0
**
pTRE-Spy1
NTA-Spy1
E
pTRE-Spy1
-siMsi1
NTA-Spy1
-siMsi1
Msi1 protein levels (IDV)
(relative to Actin)
0
-0.5
-1
-1.5
**
***
Hes1
Hes5
Log10 RQ
(relative to siControl)
0
-0.2
-0.4
-0.6
-0.8
-1
-1.2
*
*
*
pTRE-Spy1-siMsi1
NTA-Spy1-siMsi1
F
siControl
siMsi1
Symmetric mode of division (%)
80
70
60
50
40
30
20
10
0
**
*
pTRE-Spy1
NTA-Spy1

Figure 5

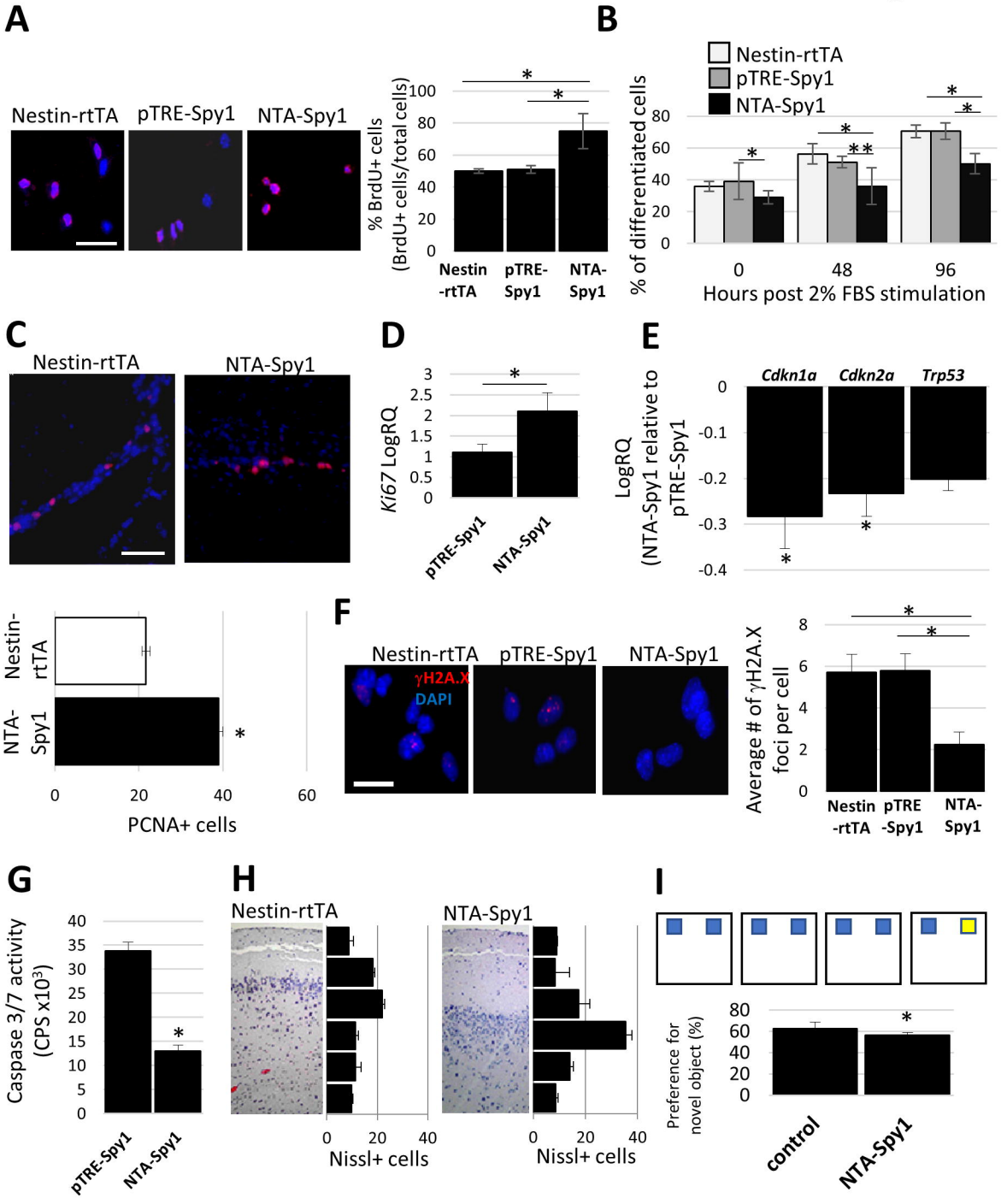
A
Nestin-rtTA
pTRE-Spy1
NTA-Spy1
% BrdU+ cells (BrdU+ cells/total cells)
Nestin -rtTA
pTRE-Spy1
NTA-Spy1
B
Nestin-rtTA
pTRE-Spy1
NTA-Spy1
% of differentiated cells
Hours post 2% FBS stimulation
C
Nestin-rtTA
NTA-Spy1
Nestin-rtTA
NTA-Spy1
PCNA+ cells
D
Ki67 LogRQ
pTRE-Spy1
NTA-Spy1
E
Cdkn1a
Cdkn2a
Trp53
LogRQ (NTA-Spy1 relative to pTRE-Spy1)
F
Nestin-rtTA
pTRE-Spy1
NTA-Spy1
γH2A.X
DAPI
Average # of γH2A.X foci per cell
Nestin -rtTA
pTRE -Spy1
NTA-Spy1
G
Caspase 3/7 activity (CPS x10³)
pTRE-Spy1
NTA-Spy1
H
Nestin-rtTA
NTA-Spy1
Nissl+ cells
Nissl+ cells
I
Preference for novel object (%)
control
NTA-Spy1

Figure 6

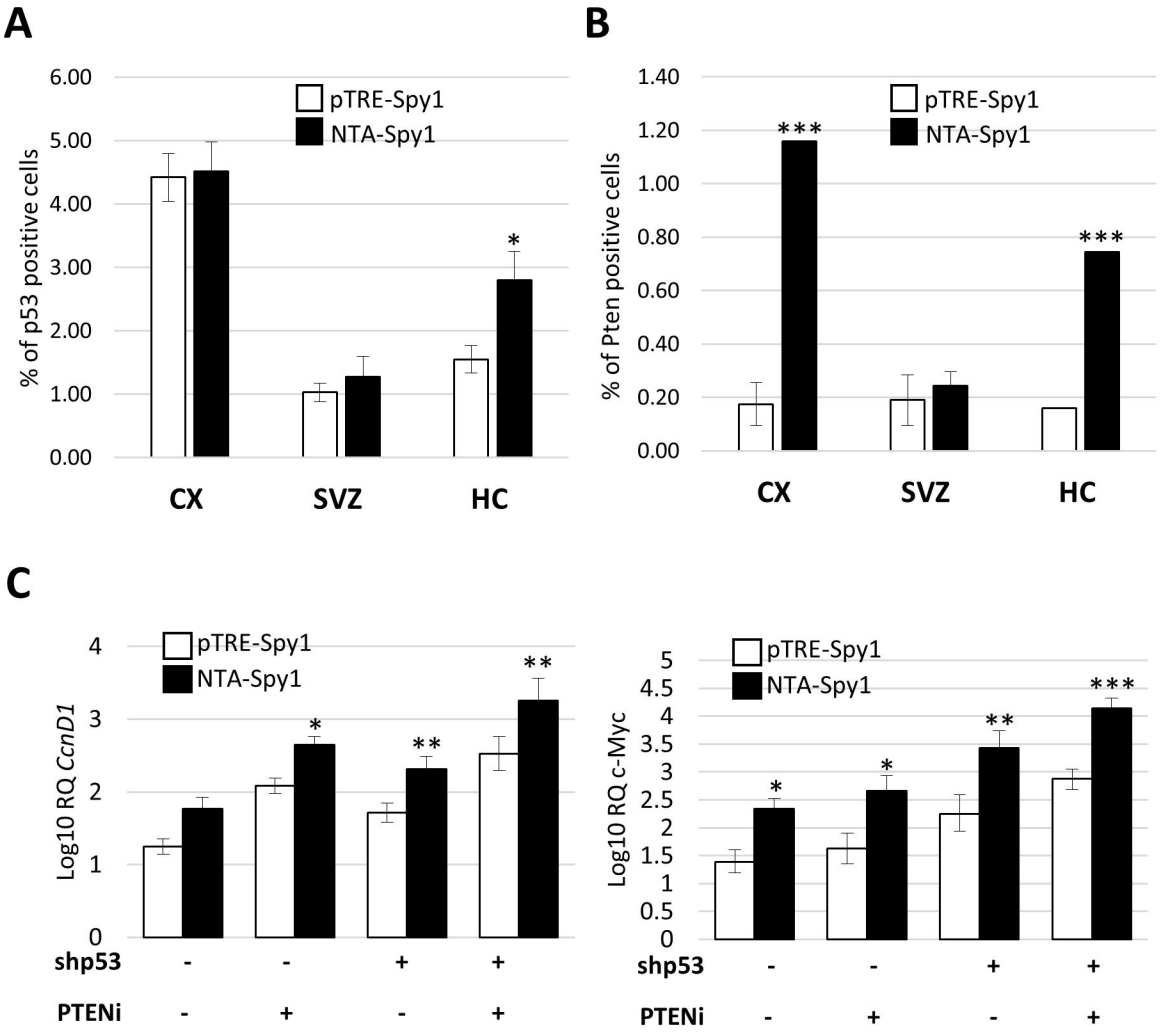
A
6.00
5.00
4.00
3.00
2.00
1.00
0.00
% of p53 positive cells
pTRE-Spy1
NTA-Spy1
*
CX
SVZ
HC
B
1.40
1.20
1.00
0.80
0.60
0.40
0.20
0.00
% of Pten positive cells
pTRE-Spy1
NTA-Spy1
***
***
CX
SVZ
HC
C
4
3
2
1
0
Log10 RQ CcnD1
pTRE-Spy1
NTA-Spy1
*
**
**
shp53 - - + +
PTENi - + - +
5
4.5
4
3.5
3
2.5
2
1.5
1
0.5
0
Log10 RQ c-Myc
pTRE-Spy1
NTA-Spy1
*
*
**
***
shp53 - - + +
PTENi - + - +

Figure 7

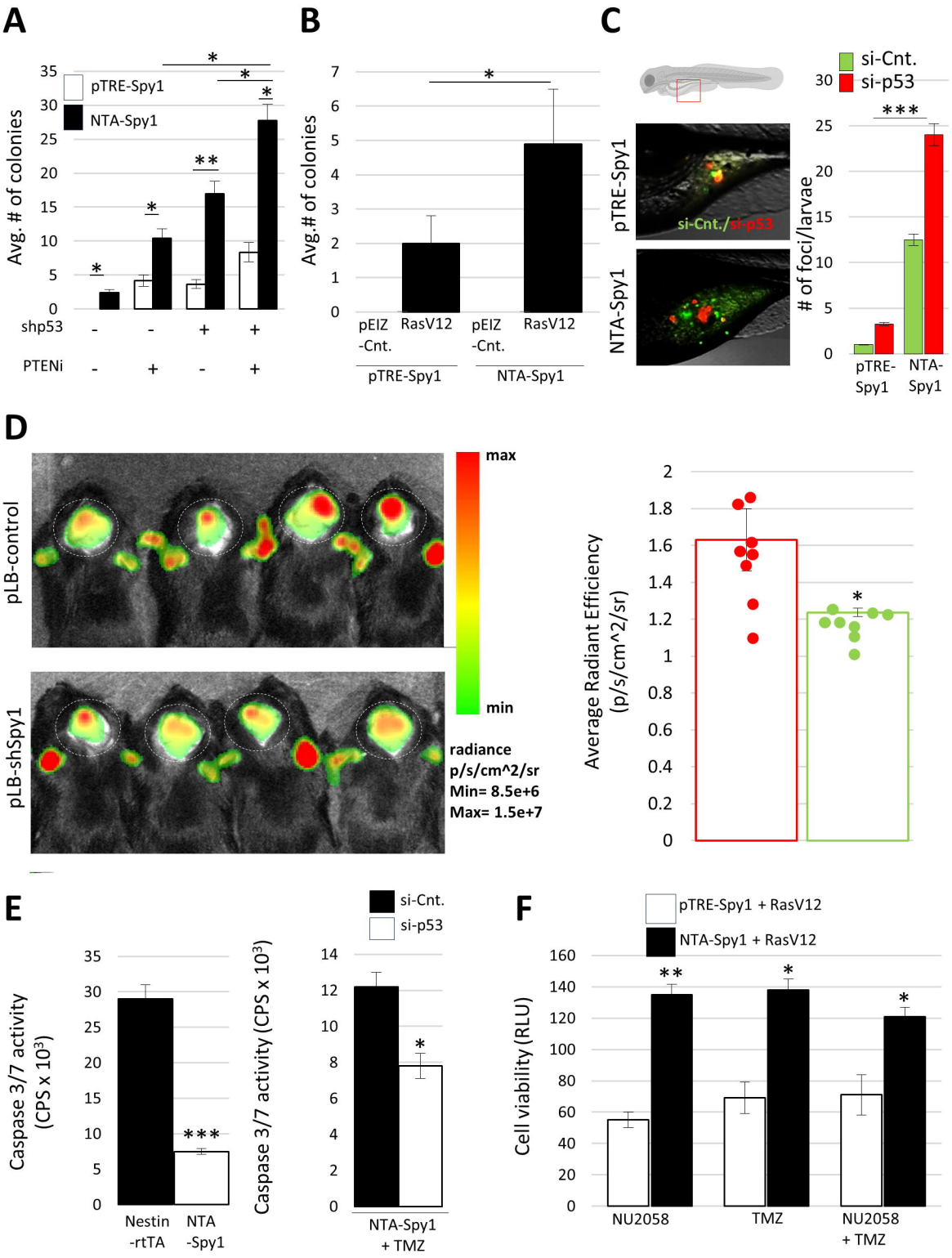
A
Avg. # of colonies
pTRE-Spy1
NTA-Spy1
shp53
PTENi
B
Avg.# of colonies
pEIZ -Cnt.
RasV12
pTRE-Spy1
NTA-Spy1
C
si-Cnt.
si-p53
pTRE-Spy1
NTA-Spy1
si-Cnt./si-p53
# of foci/larvae
D
pLB-control
pLB-shSpy1
max
min
radiance
p/s/cm^2/sr
Min= 8.5e+6
Max= 1.5e+7
Average Radiant Efficiency (p/s/cm^2/sr)
E
Caspase 3/7 activity (CPS x 10³)
Nestin -rtTA
NTA -Spy1
si-Cnt.
si-p53
NTA-Spy1 + TMZ
F
pTRE-Spy1 + RasV12
NTA-Spy1 + RasV12
Cell viability (RLU)
NU2058
TMZ
NU2058 + TMZ

Figure S1

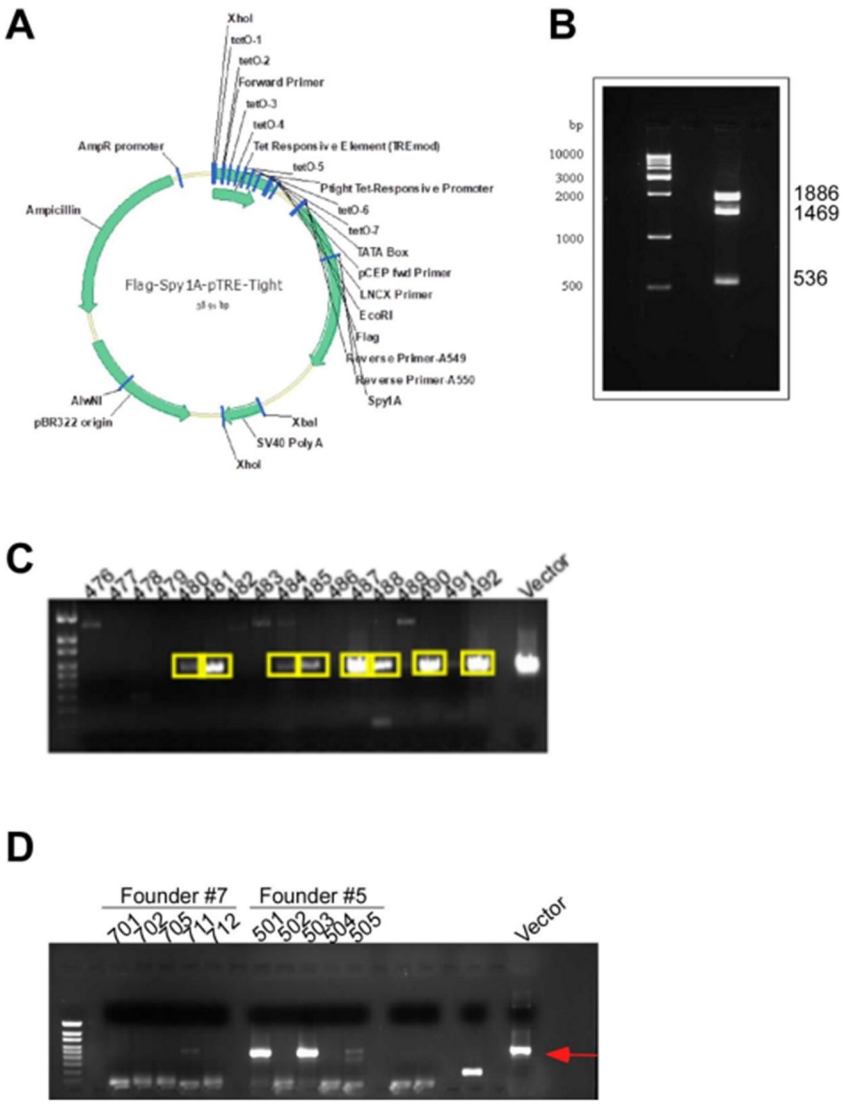
A
XhoI
tetO-1
tetO-2
Forward Primer
tetO-3
tetO-4
Tet Responsive Element (TREmod)
tetO-5
Ptight Tet-Responsive Promoter
tetO-6
tetO-7
TATA Box
pCEP fwd Primer
LNCX Primer
EcoRI
Flag
Reverse Primer A549
Reverse Primer A550
SpyIA
XbaI
SV40 PolyA
XhoI
AlwNI
pBR322 origin
Ampicillin
AmpR promoter
Flag-Spy1A-pTRE-Tight
B
bp
10000
3000
2000
1000
500
1886
1469
536
C
A76
A77
A78
A79
A80
A81
A82
A83
A84
A85
A86
A87
A88
A89
A90
A91
A92
Vector
D
Founder #7
Founder #5
701
702
705
711
712
501
502
503
504
505
Vector

Figure S2

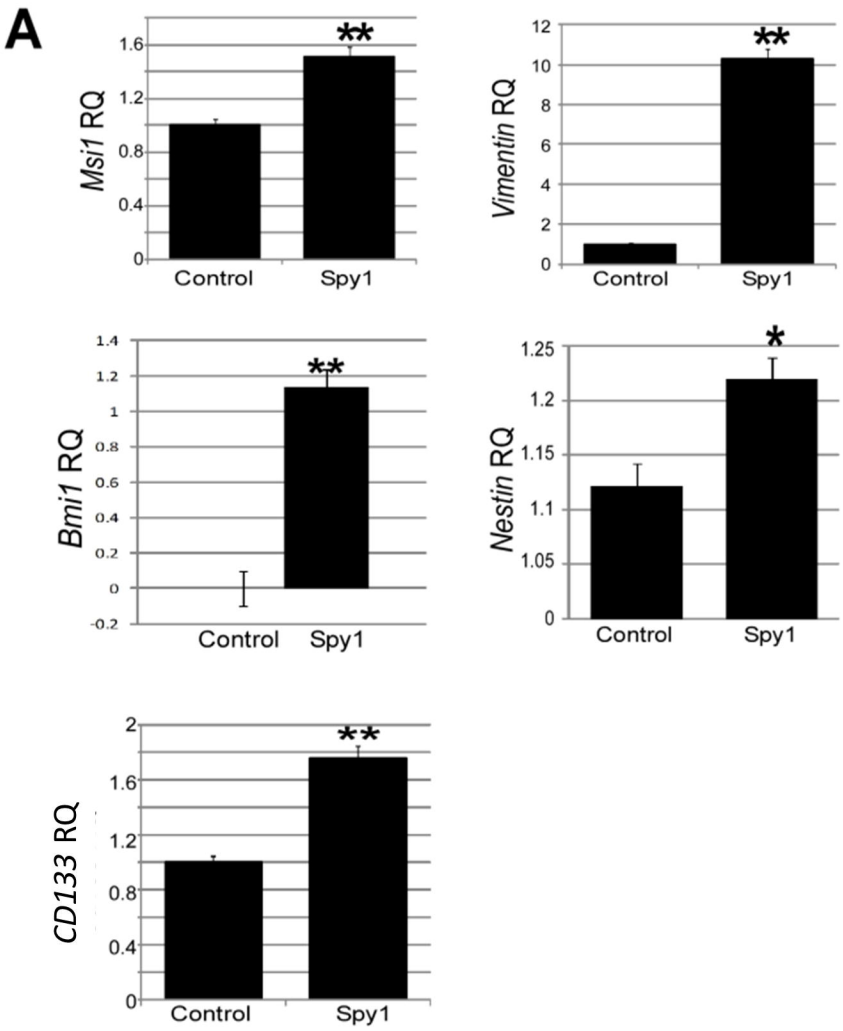
A
Msi1 RQ
1.6
1.2
0.8
0.4
0
**
Control
Spy1
Vimentin RQ
12
10
8
6
4
2
0
**
Control
Spy1
Bmi1 RQ
1.4
1.2
1
0.8
0.6
0.4
0.2
0
-0.2
**
Control
Spy1
Nestin RQ
1.25
1.2
1.15
1.1
1.05
0
*
Control
Spy1
CD133 RQ
2
1.6
1.2
0.8
0.4
0
**
Control
Spy1

Figure S3

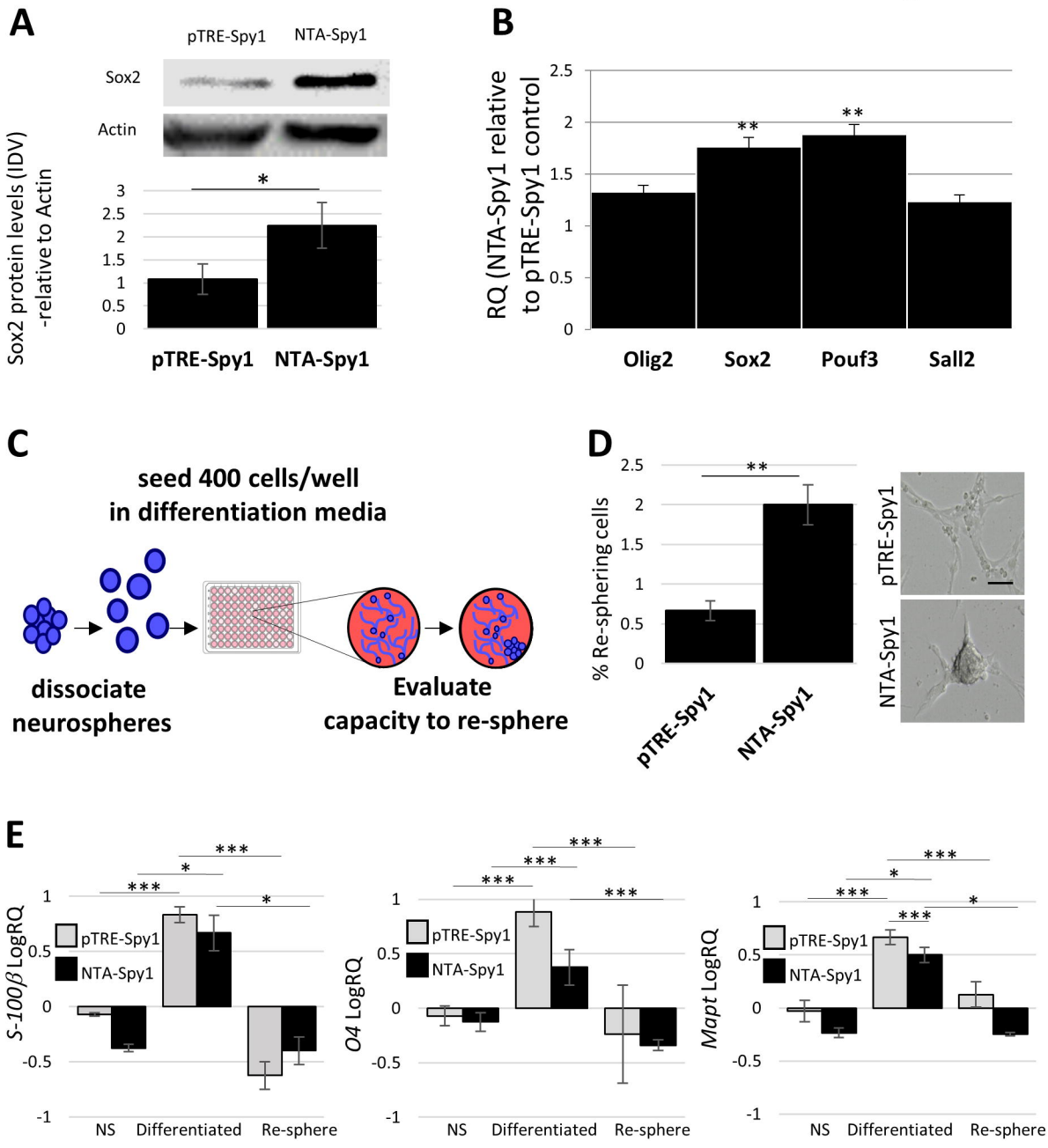
A
pTRE-Spy1
NTA-Spy1
Sox2
Actin
Sox2 protein levels (IDV) -relative to Actin
*
pTRE-Spy1
NTA-Spy1
B
RQ (NTA-Spy1 relative to pTRE-Spy1 control
**
**
Olig2
Sox2
Pouf3
Sall2
C
seed 400 cells/well in differentiation media
dissociate neurospheres
Evaluate capacity to re-sphere
D
% Re-sphering cells
**
pTRE-Spy1
NTA-Spy1
E
S-100β LogRQ
O4 LogRQ
Mapt LogRQ
pTRE-Spy1
NTA-Spy1
NS
Differentiated
Re-sphere

Figure S4

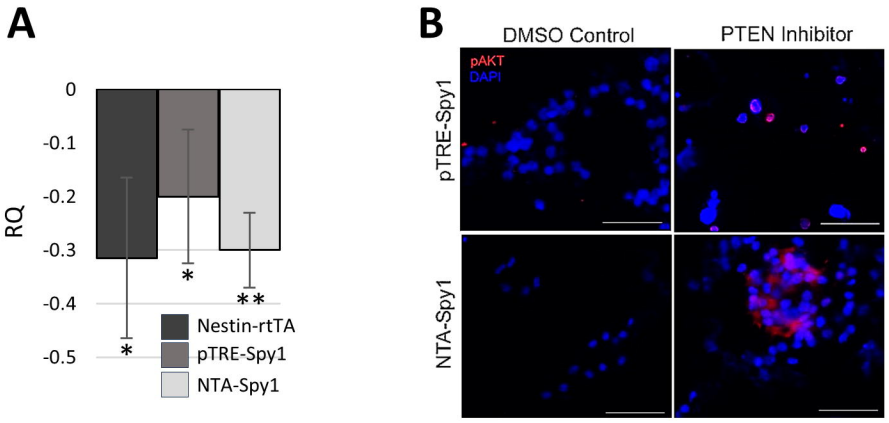
A
0
-0.1
-0.2
-0.3
-0.4
-0.5
RQ
*
**
*
Nestin-rtTA
pTRE-Spy1
NTA-Spy1
B
DMSO Control
PTEN Inhibitor
pAKT
DAPI
pTRE-Spy1
NTA-Spy1

Figure S5

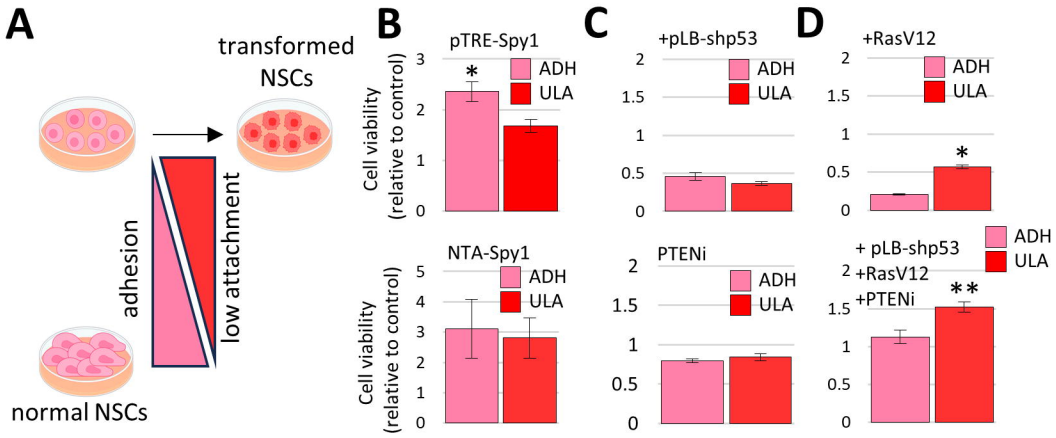
A
transformed NSCs
adhesion
low attachment
normal NSCs
B
pTRE-Spy1
Cell viability (relative to control)
ADH
ULA
NTA-Spy1
C
+pLB-shp53
PTENi
D
+RasV12
+ pLB-shp53 +RasV12 +PTENi